MICROPOLYHEDRA AND THEIR APPLICATIONS AS A CHEMICAL DISPLAY

by

Jinpyo Hong

A thesis submitted to Johns Hopkins University in conformity with the requirements for the degree of Master of Science in Engineering

Baltimore, Maryland

May 2015

ABSTRACT

Inspired by the readily observed phenomenon of self-assembly in nature, multiple self-assembling microfabrication techniques have been developed to fabricate various 3D structures in both micro and nanoscale. Among the structures that can be fabricated via self-assembly are polyhedra, an attractive model system for studying a wide range of disciplines including mathematics, chemistry and biology.

While polyhedra have been considered as an attractive model system with a wide range of implications in multiple fields of study, they are also an effective choice of encapsulant in particle technology to enable spatially controlled chemical reactions. From the formation of milk from fat globules to the development of the central nervous system (CNS) through diffusible chemoattractants, nature has benefitted from selecting and fine-tuning particles to enable spatially controlled chemistry. In past studies, scientists have mainly utilized particle technology to develop an effective system of drug delivery in micro and nanoscale.

However, the potential application of particle technology is unlimited; we were inspired to develop a novel application of a chemical display in addition to other existing applications of particle technology. We herein describe a concept of a chemical display system that can generate a dynamic pattern based on a controlled chemical release from an array of porous self-assembled micropolyhedra with various tunable properties such as dimensions, pore sizes, chemical concentrations and arrangements.

Based on the idea of controlled chemical release via particle technology, our goal is to develop a chemical display system that would be able to address an inherent limitation that exists in conventional electronic display. A concept of a chemical

display would benefit from the absence of components or interfaces that connect each pixel, allowing increased freedom in both design and utility. We fabricated our chemical display system based on an array of self-assembled micropolyhedra, a structure that can be produced in parallel at high efficiency.

In this study, we have successfully demonstrated the viability of a chemical display system by loading porous self-folded metallic cubes with chemicals and by precisely controlling the porosity, volume and chemical concentration.

We expect that our highly tunable chemical display system based on a self-assembled micropolyhedra would be able to benefit current display systems by complementing currently existing electronic displays. We also anticipate that the technology could open up new possibilities in other fields such as biotechnology, benefitting from a sequential release of chemicals, cells and more.

Advisor: Dr. David H. Gracias

Reader: Dr. Honggang Cui

ACKNOWLEDGEMENTS

Firstly, I would like to thank my family who have always provided me with unconditional love and support. I would also like to thank my brother, Ethan S. Hong, who was always with me during the tough times and helped me overcome many difficulties and hardships throughout my time in college. I cannot thank my family enough for helping me achieve a huge milestone in my life and I feel blessed to have a happy family who will always love me the way I am and whom I can always rely on.

I would also like to thank my advisor Dr. David Gracias, who gladly accepted me to his lab and allowed me to learn and explore the field of micro- and nano-fabrication under his guidance. His inspirational and impressive work and vision in micro- and nano-technology allowed me to pursue my scientific career with a strong passion and absorb a vast amount of knowledge during my time at his laboratory.

I would also like to give special thanks to Shivendra Pandey, the best mentor anyone could ask for. Under his caring guidance, I have worked on multiple exciting projects and learned to become an independent researcher. While I greatly respect him as an exceptional researcher, I still admire him more as a whole person. Working in a laboratory where things may not always work out as planned can be extremely stressful. Shivendra's constant support and kind words have been truly inspiring throughout this past year and made the tough times in research enjoyable. His compassion, maturity, and unfailing generosity of spirit make Shivendra one of the most valued and valuable person that I know of.

I would also like to thank my fellow members and the alumni of Gracias Laboratory: Hye Rin Kwag, ChangKyu Yoon, Qianru Jin, Pedro Anacleto, Tao

Deng, Evin Gultepe, Eugene Yoon, Victor Seung Hyun Oh, Tanvi Shroff, Beril Polat, and Yevgeniy Kalinin. I have thoroughly enjoyed working with them and I would have not made it this far without their help and support.

Lastly, I would like to send my sincere thanks to my dearest friends and roommates for making my 5-year-long academic journey at the Johns Hopkins University a memorable one. Also, I would like to give special thanks to a good friend of mine, Seok Kyu Kang for being a good friend and constantly providing me with a new set of perspectives to help me grow as more mature person with a deeper insight.

TABLE OF CONTENTS

TABLE OF FIGURES AND TABLES

CHAPTER 1. INTRODUCTION

1.1 Introduction to controlled chemistry and particle technology

In many contexts, chemical reactions are typically discussed based on the assumption that the reactants are well-mixed in a homogenous medium without detailed considerations on varying concentration gradients and mass transport [1]. On the other hand, non-uniform chemical reactions occurring in a heterogeneous medium are often less noticed. However, it is crucial to investigate these non-uniform chemical reactions in a heterogeneous medium; one way of doing so is by re-creating spatially controlled chemical reactions and investigating them. These spatially controlled three-dimensional (3D) chemical reactions or spatially controlled chemical patterns often offer unique properties and are known to play critical roles in many areas including various intra/intercellular processes in biological systems. For example, in *Caulobacter crescentus*, critical functions such as cell division is controlled by intracellular localization of histidine kinases and proteins based on controlled chemistry (**Figure 1a**) [2]. **Figure 1** shows other examples of chemical patterning in biological cells.
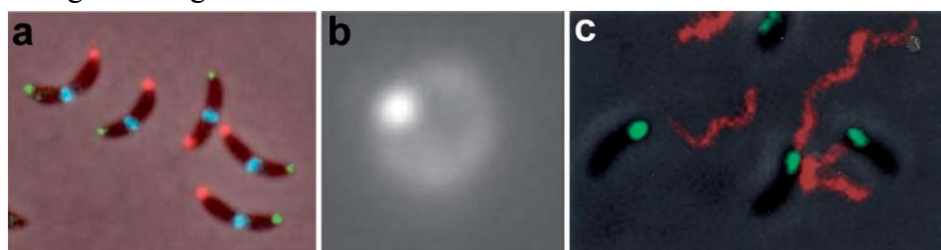
Figure 1. Examples of Chemical Patterning at in biological systems [3-5]: (a) An anterior-posterior cellular localization axis is exhibited by the Caulobacter histidine kinases PleC (red) and DivJ (green) that dynamically and selectively localize to specific cell poles. The ZapA cell division protein (blue) localizes to the FtsZ ring. (b) Live streptococcal cells (seen in the image as a diffuse ring) secrete enzymatically active SpeB at a single locus (brighter spot in the image). Representative micrograph shows that each cell displays a single punctate fluorescent locus. (c) Co-localization of expression of Eps apparatus (green) and flagellum (red) at the same pole in the cells of Vibrio cholerae. The bacteria were visualized by phase-contrast microscopy. Reprinted with permission from [1]. © 2012, RSC Advances.

To address and further investigate these spatially controlled chemical reactions, scientists have devised a way to generate a spatially controlled chemical field with patterns via a fine tuning of chemical sources. The spatial characteristics of the chemical field can be adjusted by varying different features of the chemical source, including the size, shape, chemical concentration, porosity and spatial distribution of chemical source in a medium. As a chemical source, particles with varying size and properties such as vesicles, capsules, microspheres and polyhedra can be an excellent candidate, as they can be functionalized or customized with ease [1]. Encapsulating the chemicals in these particles also allows a greater control over the rate of chemical release as well.

While most of the customizable synthetic particles that are currently available have been developed for different applications such as drug delivery, they can be utilized for the generation of spatially controlled chemical patterns. These include thin shells of molecular membranes (vesicles), capsules, polymer microspheres, polyhedra, matrices and more [1]. Among the different classes of particles, scientists can benefit the most from the lithographically patterned self-assembled polyhedra in developing a spatially controlled chemical field with favorable properties such as highly tunable and versatile nature that allows a precise control of chemical reactions and a highly parallel production process.

Utilizing spatially controlled chemistry via particle technologies can offer wide variety of applications in many areas, including drug delivery, biotechnology, chemical kinetics, reaction diffusion systems, chemotaxis and morphogenesis [1]. Our laboratory have been working extensively with polyhedra in past studies and we will work with polyhedra to develop a chemical display system based on spatially controlled chemistry in this study, which will be discussed in Chapter 3.

1.2 Introduction to polyhedra

Originating from the combination of Greek word poly (many) and hedron (base), a polyhedron (polyhedra in plural form) can be described as a three-dimensional shape with straight edges and sharp vertexes. Since Classical Greece, polyhedra have always been a source of intellectual interest and their popularity have continued for years. While their practical applications may not seem too evident at first glance, understanding the principle behind their construction and patterns have contributed to advancements in several field of study in many ways and will continue to do so in the future.

Although there numbers of different categories that consist the world of polyhedra, polyhedra can be divided into two main categories: Platonic solids and Archimedean solids. The Platonic polyhedra, named after a mathematician named Plato, is a group of convex polyhedra with identical regular polygons as their faces with all of the vertex angles being equal [6]. Platonic solids, also known as regular polyhedra in some cases, have five different types as shown in **Figure 2**. Due to their highly ordered and symmetric nature, Platonic solids have been extensively studied by mathematicians and researchers and have been of main interest.
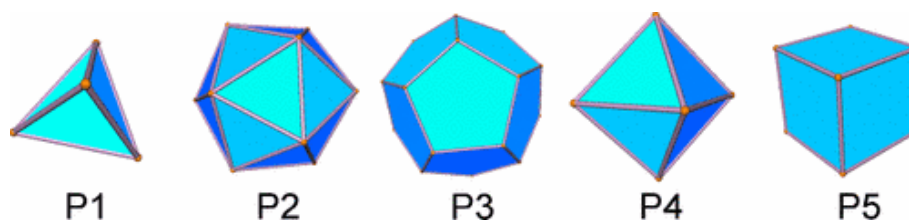
Figure 2: The five Platonic solids: Tetrahedron (P1), isocahedron (P2), dodecahedron (P3), octahedron (P4), and cube (P5). Reprinted with permission from [7]. © 2009, American Physical Society.

Apart from the Platonic solids, the other major group of polyhedra is called Archimedean solids, named after a mathematician named Archimedes. While its definition may vary, Archimedean solids are perceived as Platonic solids with a lower

degree of regularity and can be defined as a group of convex polyhedra with varying

kinds of regular polygon faces joining in identical vertices [9]. Archimedean solids,

also known as semi-regular polyhedra in some cases, have thirteen different types as

shown in **Figure 3**.
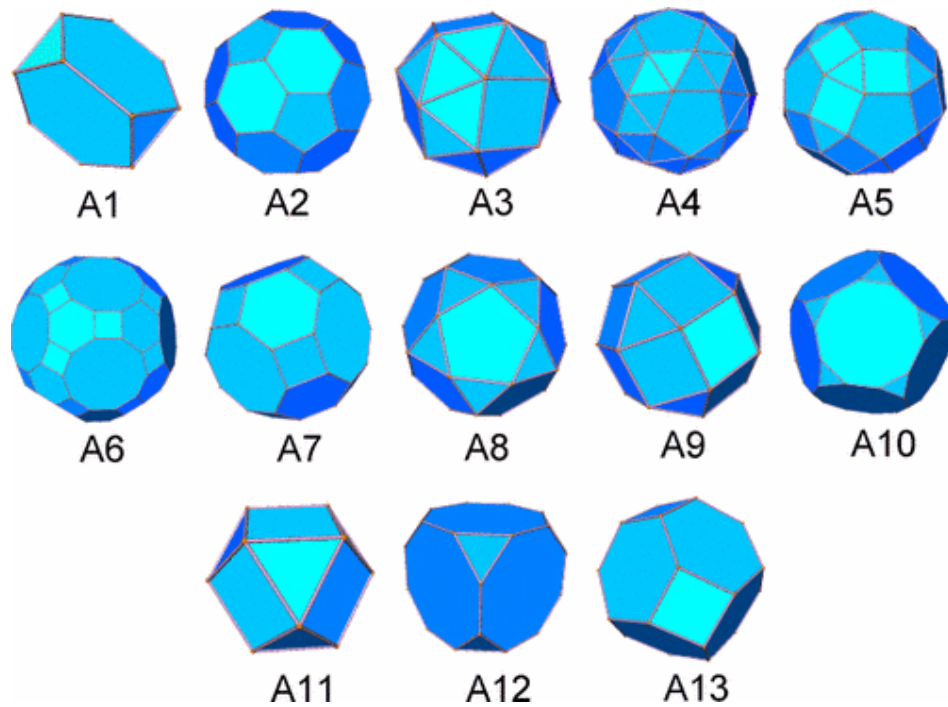
Figure 3. The 13 Archimedean solids: Truncated tetrahedron (A1), truncated icosahedron (A2), snub cube (A3), snub dodecahedron (A4), rhombicosidodecahedron (A5), truncated icosidodecahedron (A6), truncated cuboctahedron (A7), icosidodecahedron (A8), rhombicuboctahedron (A9), truncated dodecahedron (A10), cuboctahedron (A11), truncated cube (A12), and truncated octahedron (A13). Reprinted with permission from [7]. © 2009, American Physical Society.

Archimedean solids share multiple properties with Platonic solids, such as having

convex polygon as faces, straight edges and more. They can also be produced by

truncating the Platonic solids [9]. While Archimedean solids have not gained much

attention, scientists have kept a close eye on them as they are closely related to

Platonic solids. In addition to Platonic solids and Archimedean solids, there are also

other types of polyhedra such as prisms and anti-prisms that are less studied.

1.3 Polyhedra in nature and science: an attractive model system

Apart from their fascinating physical shape that sparks intellectual interest, polyhedra have always existed virtually everywhere in our lives and influenced the way people live. For decades, polyhedra have been related to a wide range of disciplines including philosophy, mathematics, chemistry, biology and physics and more [6].

Firstly, famous astronomoers and philosophers have made use of polehedra in the theories of the universe. Several decades ago, Plato associated with the five Platonic solids with the four Empedoclean elements and the universe in an effort to explain the properties of matter [8]. In addition, German astronomer Johannes Kepler utilized polyhedra to determine the size of the known universe, and the relative distances of the planets [8].

More importantly, polyhedra can be found everywhere in nature. Scientists believe that nature has benefitted from the structural stability and efficient packing that polyhedra offer. Noting this, scientists have identified polyhedra as a highly efficient building blocks of various structures, such as spherical virus (**Figure 4**), honeycomb, and even foams (**Figure 5**).
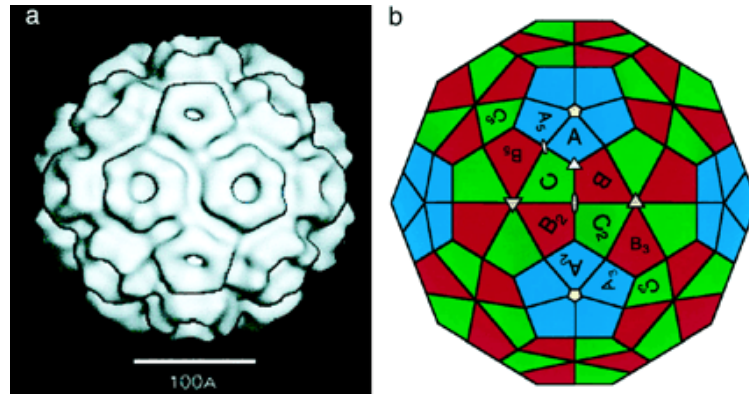
Figure 4. Polyhedra in Spherical Viruses: Cowpea Chlorotic Mottle Virus (CCMV). Icosahedral symmetry of a viral capsid. (a) Cryo-TEM reconstruction of CCMV. (b) Arrangement of subunits on a truncated icosahedron; A, B and C denote the three symmetry nonequivalent sites. Reprinted with permission from [10]. © 2004 Proceedings of the National Academy of Sciences, USA.
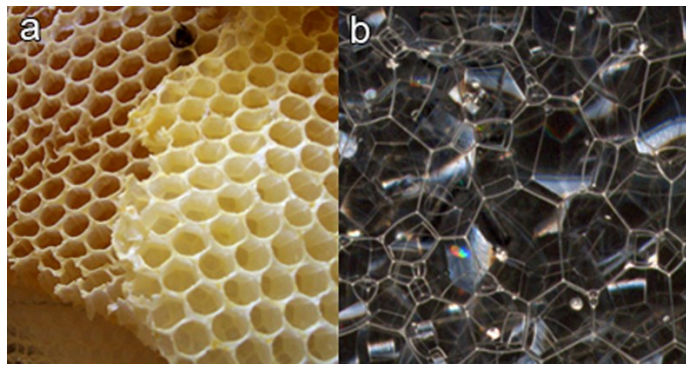
Figure 5. Polyhedra in nature. (a) Hexagonal honeycomb structure. Reprinted with permission from Merdal [CC-BY-SA-3.0]. (b) Packing of foam cells from a variety of polyhedra. Reprinted with permission from André Karwath [CC BY-SA 2.5].

As a very attractive model system, polyhedra have drawn significant attention and scientists have spent much effort in understanding and characterizing the packing of polyhedral shapes as a result. With their significance, it is expected that a further investigation on polyhedra can contribute greatly to an understanding of complex problems such as the topology of cells, grains, polycrystals and other three-dimensional microstructures [11].

6

While polyhedra have been studied extensively for years, the progress in research on polyhedra has been quite slow. However, with a recent revolution in fabricating techniques of 3D structures, working with microscale polyhedra has become more accessible and a rising tide of research on polyhedra is expected. Currently, a variety of research on polyhedra is ongoing in multiple fields of research, including algebraic geometry, mathematical programming, computer graphics, combinational optimization, topology, crystallography, VLSI design, robotics and more [12].

1.4 Limitations of conventional techniques for the fabrication of 3D structures

Although the potential of structures in micro and nanoscale was noted for decades (see the American physicist Richard Feynman's lecture titled "There's Plenty of Room at the Bottom" in 1959), the fabrication of these structures was very difficult until various microelectromechanical systems (MEMS) microfabrication techniques started to emerge. Currently available techniques that are used to fabricate microscale structures can be classified into three broad categories: bulk machining, surface machining and LIGA methods (German acronym for 'Lithography', 'Electroplating' and 'Molding') [13].

While currently available microfabrication techniques based on processes such as photolithography and etching can be used to synthesize various structures in microscale, their utility is largely limited in the synthesis of a 2D structure [14].

An example of such techniques is surface micromachining, a well-developed method that is one of the major fabrication techniques for 2D and 3D microscale structures and devices. In surface micromachining, multiple layers of films with different materials are deposited as structural and sacrificial materials then etched upon patterning for the production of microstructures [13,15]. In the process, sacrificial layers are first deposited onto the substrate in order to protect and maintain subsequent layers onto which

a structural layer will be deposited. Then, thin layers of structural layers are deposited

which will then undergo selective patterning and etching. Finally, the remaining

sacrificial layer will be removed, leaving only the desired structure [13]. A typical

fabrication process in surface micromachining is outlined in **Figure 6.**
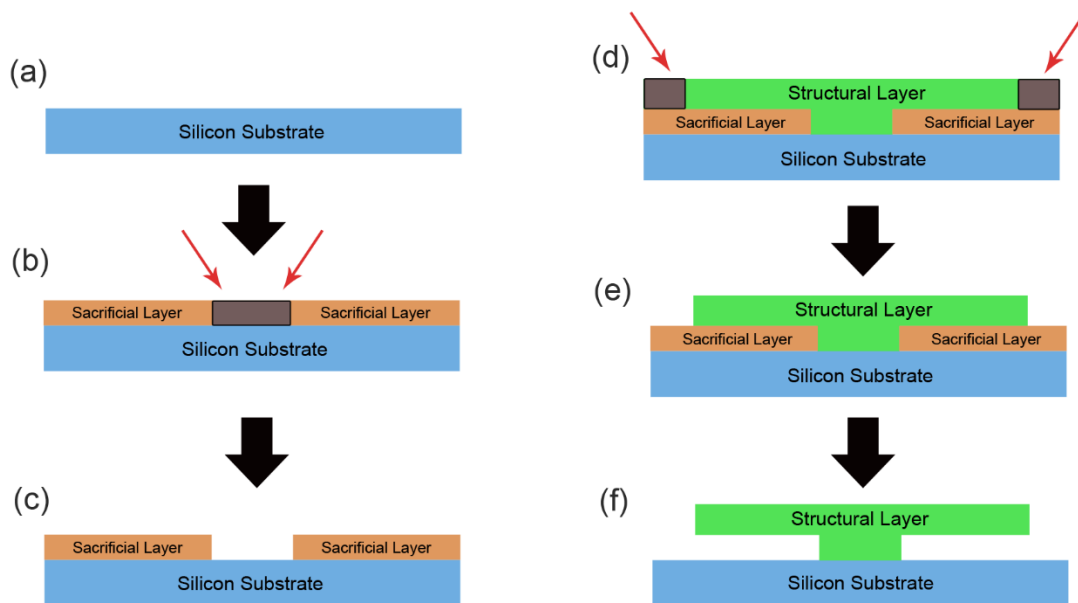
Figure 6. Process flow for surface micromachining fabrication. (a) Deposition of the sacrificial layer on a silicon substrate. (b) Etching of the sacrificial layer after patterning. (c) Deposition of a layer for the structure material. (d) Etching of the structural layer after patterning. (e) Final etching of the sacrificial layer. (f) Final product with structural layer only.

Also called a thin film process, surface micromachining allows the fabrication of

3D microdevices along with the production of electronic integrated circuit (IC) devices

[15]. However, with limitations on each film's thickness, the production of 3D structure

and devices is largly limited to planar-type and does not allow fabrication of complex 3D

structures such as polyhedra or hollow rods [18]. As shown in **Figure 7** below, typical

structures and devices fabricated by micromachining fabrications are mainly planar

structures such as sensors, microchannels and cantilevers. In addition, although surface

micromachining allows the production of precise and versatile structures, it has limited

range of materials that can be used at a relatively high production cost [16].
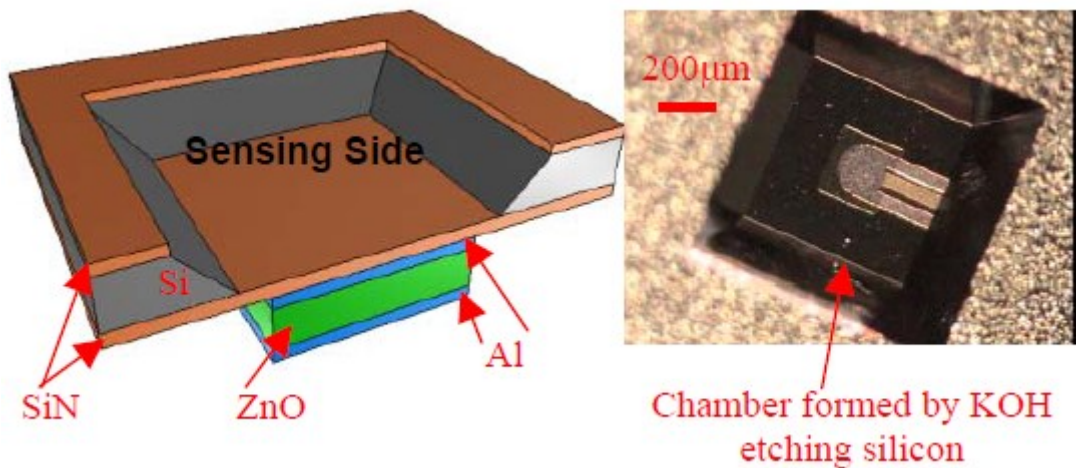
Figure 7. Resonant mass sensors based on film Bulk Acoustic Resonator (FBAR) produced by micromachining process. (Left) Schematic of an FBAR. (Right) Photo of a fabricated FBAR sensor. Reprinted with permission from [22]. © 2011 IEEE.

Apart from the traditional microfabrication techniques mainly based on photolithography, other microfabrication techniques still suffer from issues such as the pattern resolution and the flexibility of geometry [16]. These techniques include injection molding, imprinting, cast molding, screen printing and more [18-22].

1.5 Introduction to self-assembly

As discussed above, many of the traditional microfabrication techniques do not perform particularly well when it comes to the fabrication of 3D micro and nanostructures with numbers of limitations. To address the inherent limitations in the production of 3D structures found in the majority of microfabrication techniques, scientists looked for solutions. Finally, they were able to get a clue from our nature; the answer lied in the phenomenon of self-assembly.

While its definition varies, self-assembly can be defined as "a process in which components, either separate or linked, spontaneously form ordered aggregates [23]." In nature, self-assembly occurs in a wide range of length, including both molecular scale and macroscale. Self-assembly accounts for thousands of phenomenon in nature; it includes

9

the self-arrangement of sand dunes from thousands of individual dust particles and the self-assembly of nanoscale biological structures such as virus and DNA molecules. **Figure 8** illustrates some examples of self-assembled the biological structures.
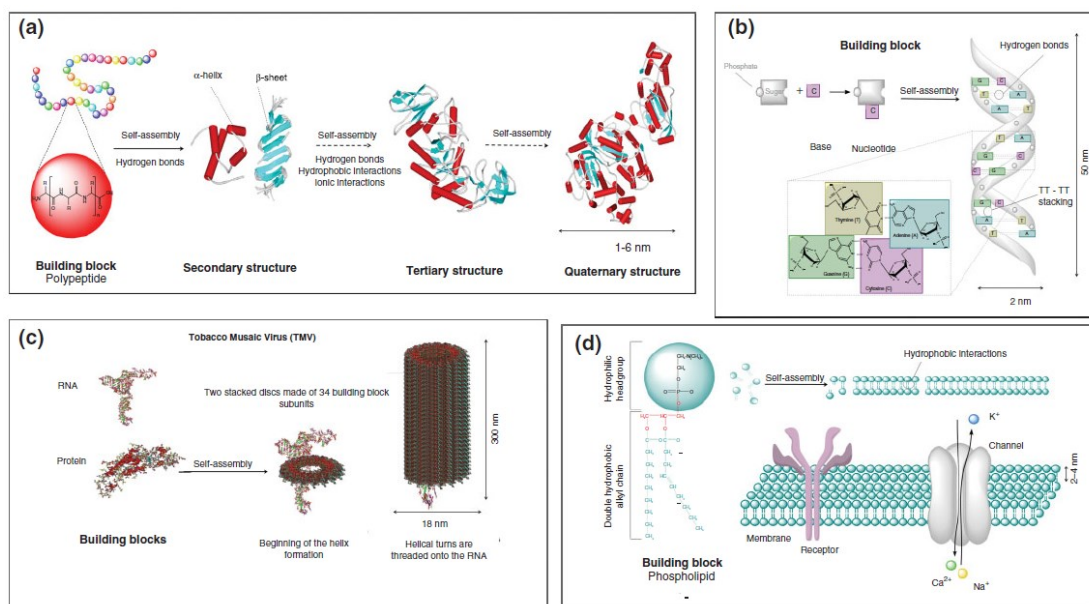
Figure 8. Examples of biological self-assembled structures showing the building blocks and the relevant interactions involved in the self-assembly process. (a) Protein folding. (b) ds-DNA. (c) Tobacco mosaic virus (TMV). (d) Cell membrane. Reprinted with permission from [24]. © 2013 John Wiley and Sons.

As self-assembly is ubiquitous in various fields of study such as chemistry, biology and materials science, numbers of research have been made in self-assembly in the past [23]. Although studying self-assembly will benefit these fields of study as a whole, one of the most important applications of self-assembling process is found in the fabrication of 3D structures in nano and microscale. This is because self-assembly offers "routes to ordered states of matter that probably cannot be generated practically by any other type of processes [and] has specific applications in materials science and engineering [23,25]." Self-assembly allows not only an efficient route to fabricate complex 3D microstructures but also a possible assembly of nanoscale components, which is often an extremely difficult process. **Figure 9** illustrates some examples of self-assembled 2D and 3D structures.

10
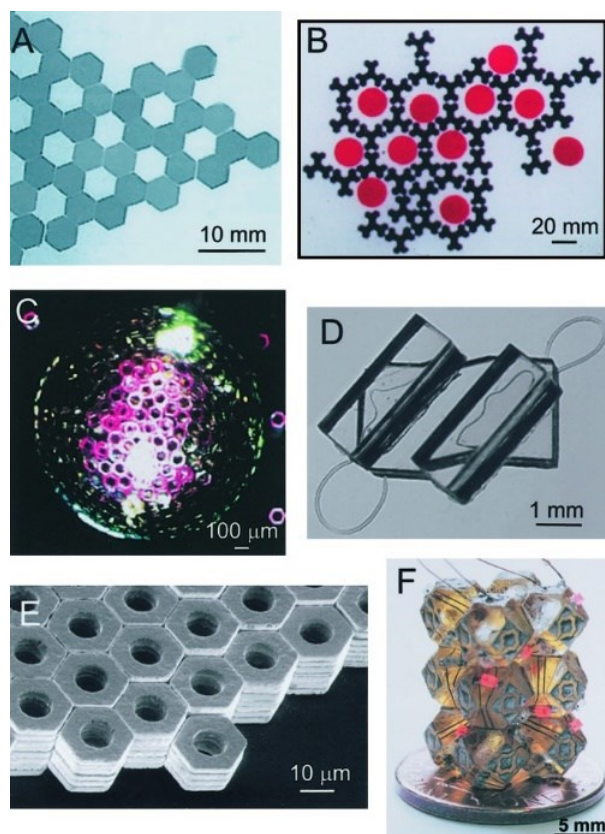
Figure 9. Examples of 2D (A and B) and 3D (C-F) structures, assembled in systems of macroscopic components interacting via capillary interactions [23, 26-31]. (a) Open hexagonal array. (b) Hexagonal lattice formed around circular templates. (c) Spherical structure formed by self-assembly of hexagonal metal plates. (d) Compact 3D structure formed by self-folding of a string if tethered, polymeric polyhedra. (e) Large crystal self-assembled from micrometer-sized hexagonal metal plates. (f) Aggregate with electrical connectivity self-assembled from polyhedral, polymer components. Reprinted with permission from [23]. © 2002 Proceedings of the National Academy of Sciences, USA.

With their strong potential and increasing interest, self-assembly based microfabrication techniques are expected to open up new opportunities in fabricating highly functional structures in both micro and nanoscale. We hereinafter focus on the fabrication of microscale 3D structures based on self-assembling processes in the following chapters.

CHAPTER 2. SELF-FOLDING POLYHEDRA

2.1 Introduction to self-folding approach in self-assembly

Although an efficient, high-volume production of patterned planar 2D structures is readily available using conventional microfabrication techniques, the fabrication of precisely patterned 3D structures is still very challenging. By combining current lithography techniques with self-folding approach, however, a production of complex 3D structure is possible by folding planar 2D templates structures into 3D structures. The result is a highly parallel fabrication process of precisely patterned and complex structures such as polyhedra.

In the context of self-assembly, self-folding broadly refers to the process in which interconnected "planar structures fold up spontaneously, typically when released from a substrate or exposed to specific stimuli [32,33]." The resulting product are complex 3D structures such as polyhedral, cylindrical tubes, spirals and corrugated sheets that are otherwise hard to fabricate using other approaches [32].

The concept of self-folding can be seen as a "more deterministic form of self-assembly" where components are linked in a specific way in order to reduce the degrees of freedom and guide the interactions between the components in order to achieve a "guided assembly of a pre-determined 3D structure [34]. " **Figure 10** gives an example of an approach in developing different methods in the self-folding process of different structures.
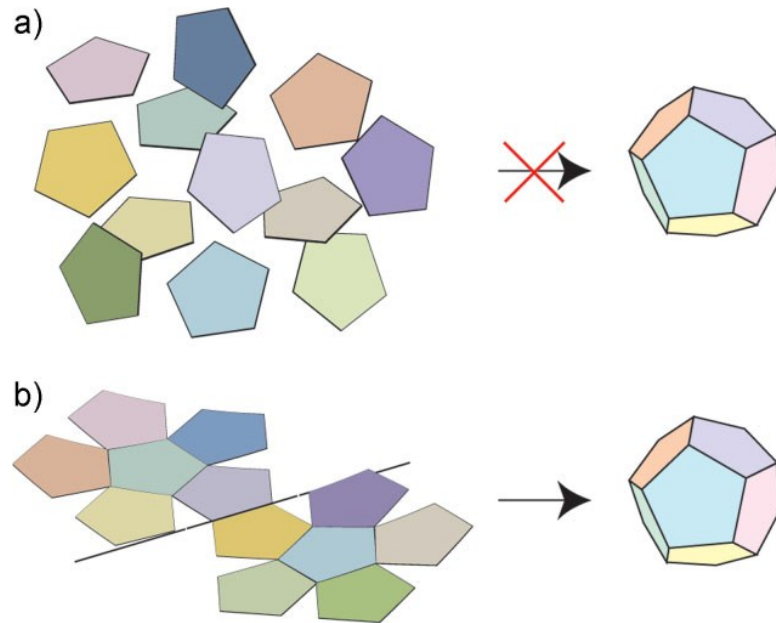
Figure 10. Variations on the self-assembly theme. (a) It is highly improbable that 12 free-floating pentagonal panels will self-assemble to form a hollow dodecahedron. (b) Tethering limits the number of possible self-assembly outcomes and can be used to construct a hollow dodecahedron with higher probability. Reprinted with permission from [34]. © 2010 John Wiley and Sons.

Currently, there are multiple mechanisms to enable self-folding. These include magnetic forces, pneumatics, swelling of electro-active polymers, ultrasonic pulse impact, stressed thin films, surface forces and more [34]. **Figure 11** shows the implementation of these self-folding techniques with various 3D microstructures as the product.
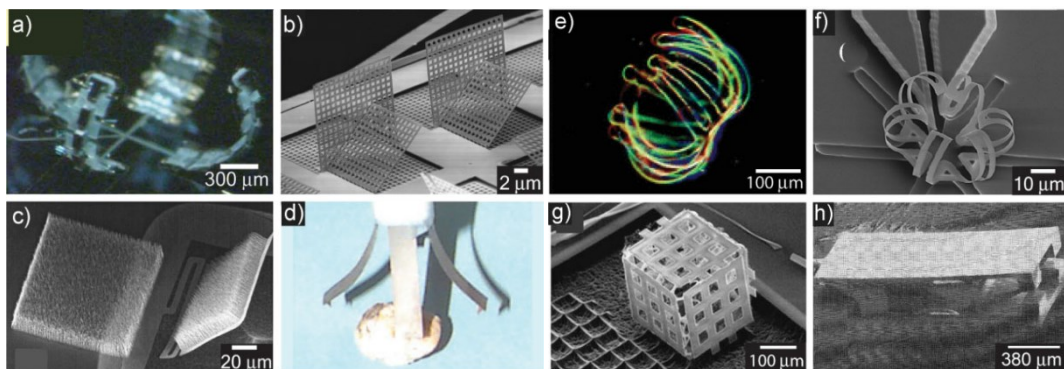
Figure 11. Implementation of various self-folding techniques [24, 35-41]. (a) Pneumatically actuated microhand. (b) Magnically assembled microstructures with elastic hinges. (c) TiN membrane folded due to the stress in TiN hinge. (d) End gripper made of ionic polymer-metal composites. (e) 3D microwell self-folded from a hydrogel bilayer. (f) SU8/DLC normally-closed microcage folded by residual stress. (g) Microcube fabricated using thermal shrinkage of polyimide. (h) SMA-actuated microgripper. Reprinted with permission from [34]. © 2010 John Wiley and Sons.

2.2 Fabrication of the surface tension driven self-folding polyhedra

Among the several strategies to facilitate self-folding in the self-assembly of 3D structures, the utilization of surface forces has become one of the most preferred method for self-folding due to its several advantages over the other approaches.

First of all, the surface-tension driven self-assembly is a very appealing and versatile production method as it does not require active actuation [42]. In addition, in the surface-tension driven assembly, the surface force scales linearly with the characteristic length and the gravitational force scales with the length cubed. This means that the interfacial force will dominate at smaller length scales instead of the gravitational force, thereby allowing the assembly of 3D structures over a wide range of sizes from nano to microscale [29,38].

The surface force or tension involved in the surface-tension powered self-assembly is produced when each meltable surface of a 2D planar template tries to minimize its interfacial free energy by minimizing its surface area. The process of surface tension driven self-assembly begins with the production of the 2D template, where a movable panel is attached to a flexible hinge. Then the meltable pad is deposited on the hinge, which will melt upon heating. Upon heating, the free surface of the hinge will deform with a decrease in surface energy that will provide the rotational torque to rotate the attached panel. The folded structure will then stabilize after a balance among the torques is achieved, with the meltable pad portion resolidifying back to the original state to give a stable folded structure [42]. The general overview of the self-assembly powered by surface tension is illustrated in **Figure 12** below.

14
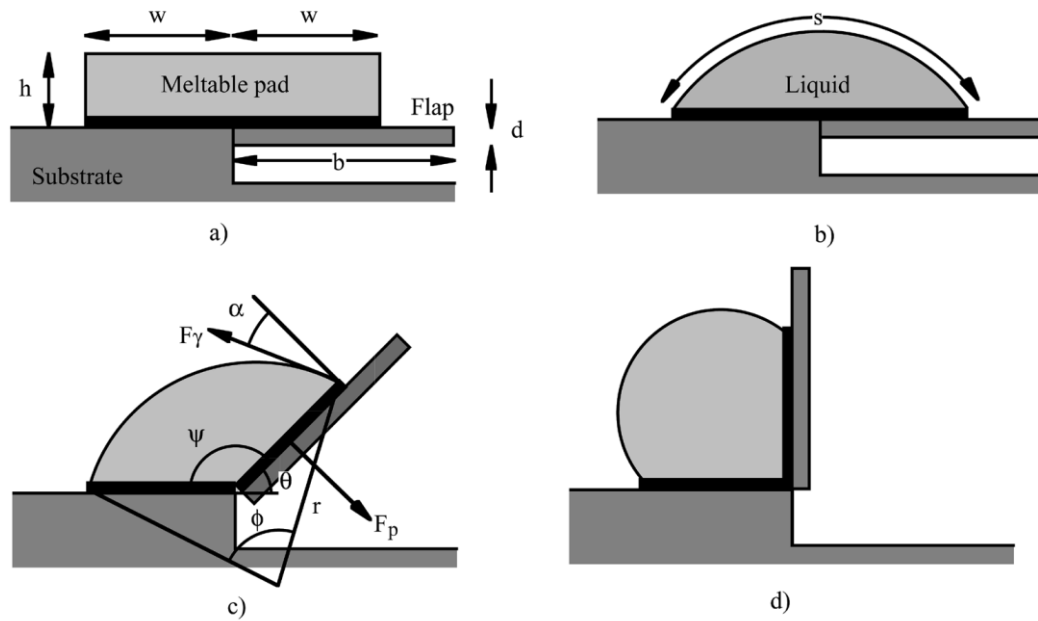
Figure 12. Rotation of panels powered by the surface tension. (a) A 2D template with a flexible hinge attached to rotatable panel deposited with a meltable pad. (b) As the meltable region starts to melt, the surface area starts to decrease. (c) The surface area of meltable pad region gets minimized as the surface tension (Fγ) and the Laplace pressure (Fp) balances to reach the equilibrium. (d) Folded hinge stabilized in the equilibrium position. Reprinted with permission from [42]. © 2003 IEEE.

By adapting the existing surface tension powered self-assembly technique and developing it further, our lab has successfully mass-fabricated various untethered, patterned polyhedral structures in microscale [34]. The additional step that allows the fabrication of untethered polyhedra based on surface tension driven self-assembly is the incorporation of sacrificial layers in the fabricating steps of 2D planar structures. In the self-assembly process, sacrificial layers get selectively removed and allow the 2D planar structure to be completely released from the substrate, which will then fold into a sealed 3D structure with fluidic locking hinges. The schematic illustration of the surface-tension driven assembly of polyhedra is shown in **Figure 13** below.
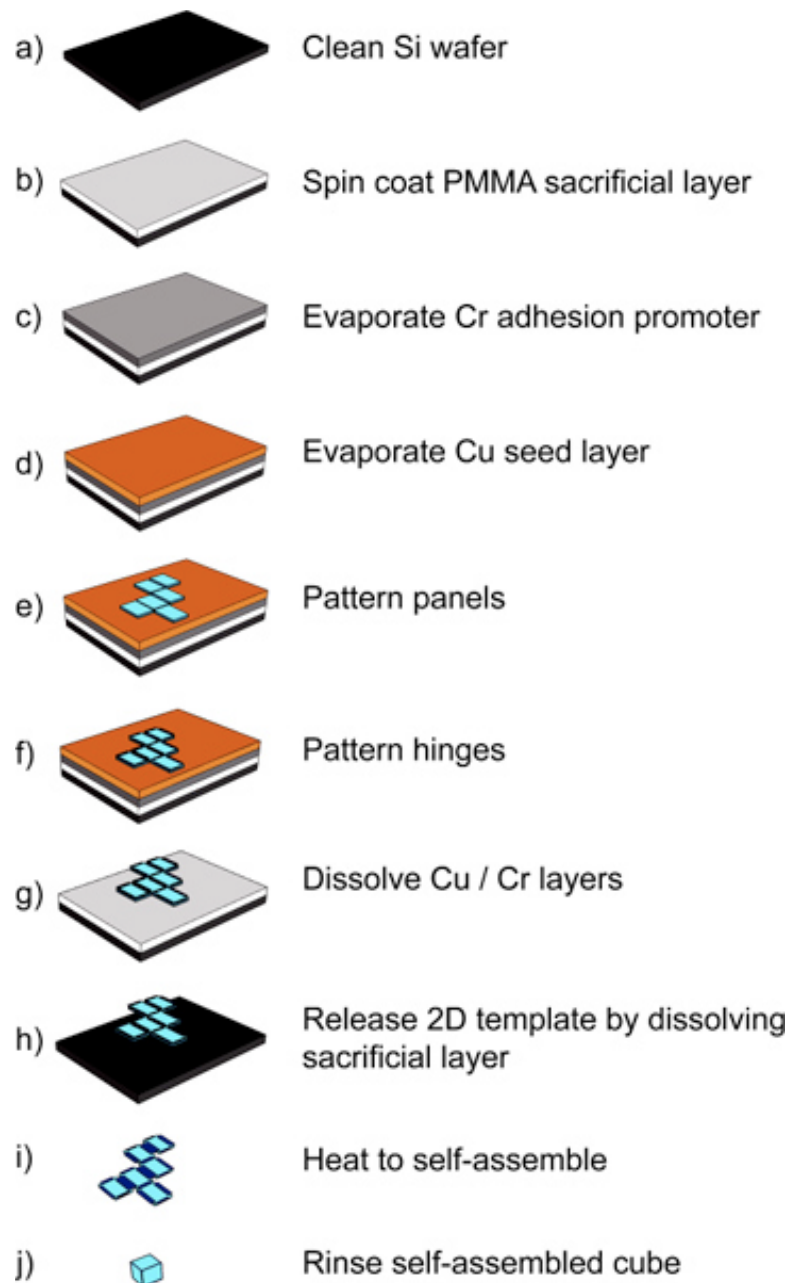
Figure 13. Schematic illustration of key fabrication steps for the surface tension driven assembly of a cubic polyhedra. Reprinted with permission from [14].

Since this fabrication method is based on previously well-developed lithographic techniques, it allows the versatility in size, shape, porosity with added functionality such as patterning. **Figure 14** shows the images of various microscale polyhedra structures fabricated from the surface tension driven self-assembly.
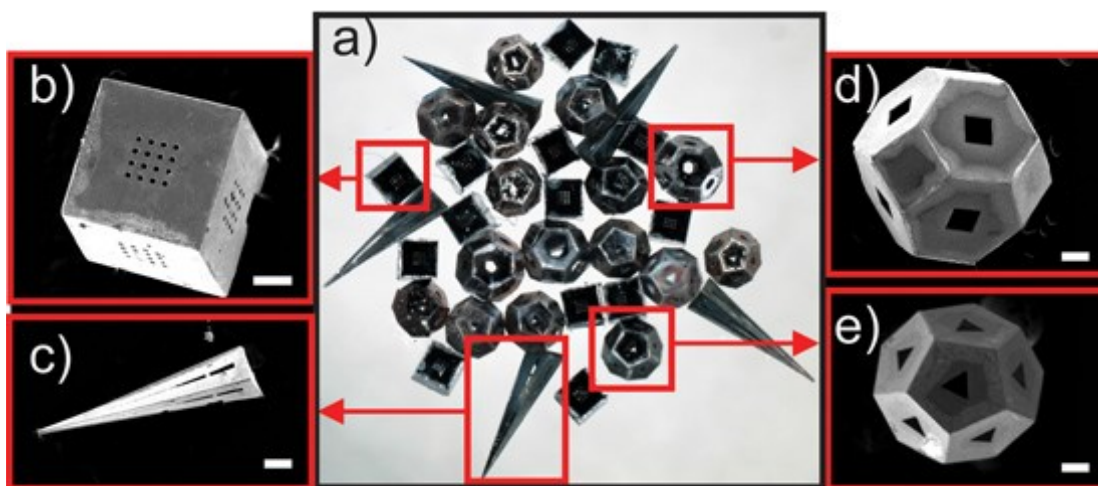
Figure 14. Surface tension driven self-assembled patterned polyhedra. (a) Optical image of self-assembled polyhedra in a variety of shapes. (b) SEM image of self-assembled porous cube. (c) SEM image of self-assembled pyramid. (d) SEM image of self-assembled truncated octahedron. (e) SEM image of self-assembled dodecahedron. Size of the scale bars are $100\mu m$. Reprinted with permission from [14].

As shown above, these versatile polyhedral structures can be fabricated into multiple shapes, added with various types of patterns in their panels with their size ranging from nanoscale to macroscale (mm). Added with a highly parallel and cost-effective manufacturing process, these polyhedral structures offer a wide range of applications in multiple fields of study.

First and foremost, due to their hollow nature, these self-assembled polyhedra can be utilized as containers. As they can be facilitated with micro and nanoscale pores, their potential use in 3D membrane for separations and sampling and controlled drug delivery have been demonstrated previously [43,44]. Since these structures can be fabricated with metallic materials based on lithography, people have also demonstrated their use in controlled chemistry and medical imaging based on external forces that can actuate these structures [45,46]. Scientists also believe that the self-assembled polyhedra may even be able to provide "a framework for building 3D electronic device modules for self-assembled electronic systems [21]."

17

While surface tension driven self-folding technique allows a highly efficient and parallel production of complex 3D structures with multiple advantages, it is not free of limitations. Because surface tension driven assembly relies on a surface curvature of liquefied metals to propel attached structures, it often requires high temperatures for the meltable hinges to melt. This requirement limits the technique's biocompatibility and therefore other mechanisms that enables self-assembly may be able to provide a better biocompatibility in biological systems. All in all, surface tension driven self-folding is a very attractive process that allows the fabrication of complex 3D structures in a highly parallel and efficient manner while retaining the benefits of existing microfabrication techniques.

2.3 Design considerations and geometric design rules of self-folding polyhedra

Although the self-folding process by surface tension is guided by the patterned structure of the planar 2D template, its yield of completely folded, defect free structure is far from being perfect. In order to address this issue, our laboratory has worked extensively with the surface tension guided self-folding process and discovered the factors that affects the folding process, developing several design rules and considerations that can be implemented to maximize yield with defect-free structure.

In their work, Leong et. al successfully developed the optimal design rules for generating 2D templates that can be used for the surface tension driven assembly of polyhedra. After observing how different dimensions of a 2D template affected the folding process, they reported that for a polyhedra with a side length of L, folding hinges should have a dimension of 0.8L $\times$ 0.2 L (length $\times$ width) while sealing

hinges should have a dimension of 0.8L × 0.1 L (length × width) [14,47]. The

schematic representation of this design rule is shown in **Figure 15**.
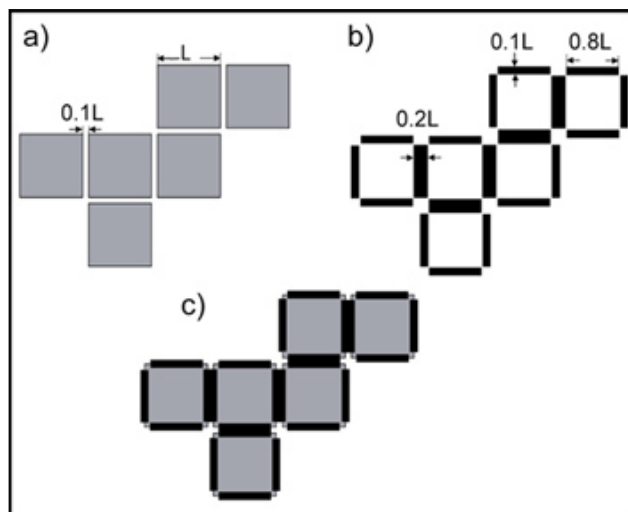
Figure 15. Mask design rules for the assembly of patterned polyhedral particles. (a)
Schematic of the panel mask for a polyhedron of side length L. (b) Schematic of the hinge mask
featuring folding hinges (0.2L×0.8L) and sealing hinges (0.1L×0.8L). (c) Schematic of the
overlaid 2D template or precursor. Reprinted with permission from [14].

In addition, they also investigated the dependence of the folding angle of a

panel on the volume of hinge material and demonstrated that the folding angle of a 2D

template decreases with an increasing volume of a hinge material, thereby effectively

controlling the folding process in self-assembly [47]. **Figure 16** illustrates the

simulation results.
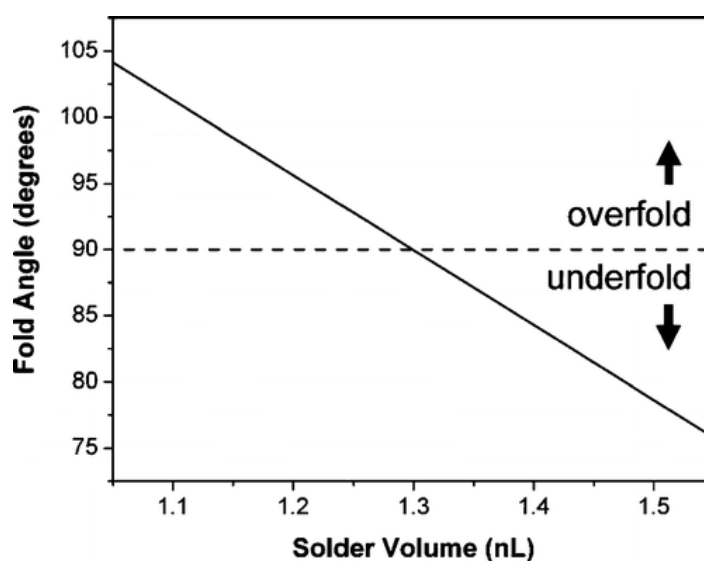
Based on this design rule, our lab has been able to mass-produce various polyhedra particles with sizes ranging from microscale to macroscale (cm). In addition to these design considerations, other studies on other principles that guide self-assembling process of polyhedra such as the investigation on the role of compactness nets for polyhedral self-assembly have been made in an effort to gain a better understanding of self-assembly process with improved yield [48]. **Figure 17 and 18** illustrate Pandey et al.'s findings that "compactness is as simple and effective design principle for maximizing the yield of self-folding polyhedra" [48].
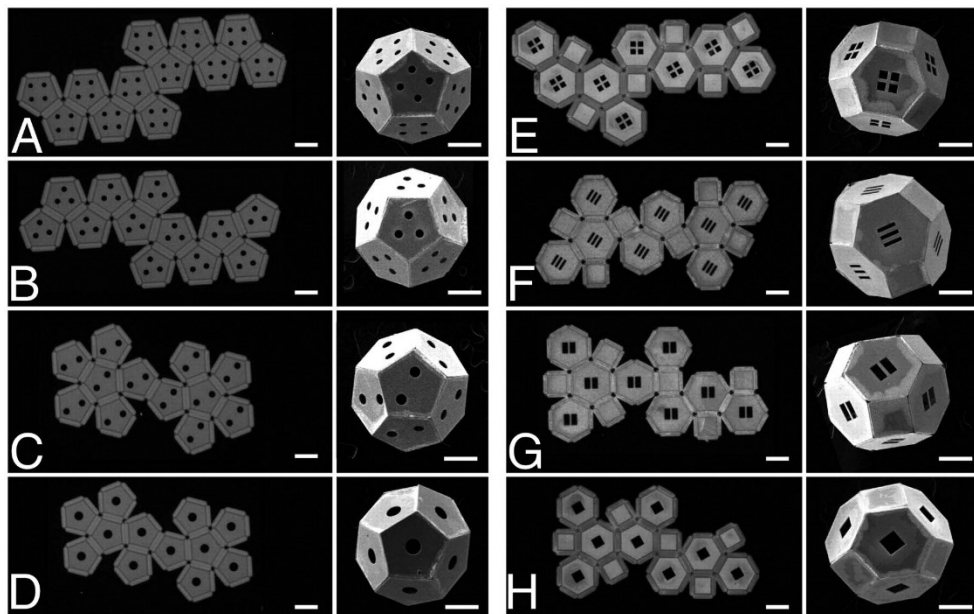
Figure 17. Self-folding experiments on high Vc (total number of distinct vertex connections) nets with varying Rg (radius of gyration). Optical and SEM images. (A–D) Dodecahedral nets with $Vc = 10$ and $Rg = 810.2, 797.4, 755.4,$ and 747.7 μm, respectively. (E–H) Truncated octahedral nets with $Vc = 12$ and $Rg = 911.6, 870.2, 867.4,$ and 852.8 μm, respectively. (Scale bar: 300 μm.) Reprinted with permission from [48]. © 2011 Proceedings of the National Academy of Sciences, USA.
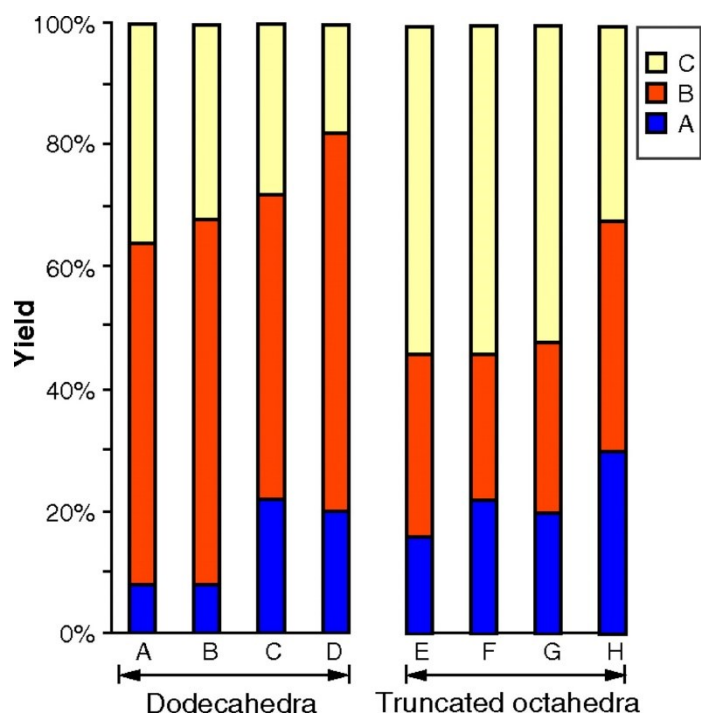
Figure 18. Self-folding experiments on high *Vc* (total number of distinct vertex connections) nets with varying Rg (radius of gyration). Optical and SEM images. (A–D) Dodecahedral nets with $Vc = 10$ and $Rg = 810.2, 797.4, 755.4$, and 747.7 μm, respectively. (E–H) Truncated octahedral nets with $Vc = 12$ and $Rg = 911.6, 870.2, 867.4$, and 852.8 μm, respectively. (Scale bar: 300 μm.) Reprinted with permission from [48]. © 2011 Proceedings of the National Academy of Sciences, USA.

As shown in Figure 16 and 17, Pandey et al. reported that by adjusting *Vc* (total number of distinct vertex connections) and varying Rg (radius of gyration), the two factors that measure the metric and topological compactness of a structure, can result in a high yield of defect-free self-assembled structures [48].

CHAPTER 3. A CHEMICAL DISPLAY BASED ON POLYHEDRA[*]

3.1 Introduction

While currently available electronic display system such as liquid crystal displays and flexible displays is being widely used, fundamental limitations lie in its utility and design exist due to their design in nature: the wired interface that connects individual pixels [45,46]. Because the information to be displayed in electrical display needs to be transmitted through wired interfaces, the wired interface is required in the majority of conventional electronic visual display, with the exception of recently introduced wireless display [45-49]. As a result, the internal design of electronic display becomes increasingly complex due to multiple interconnecting components with the need for external power source to operate the display; the utility of these devices can be limited [55].

Based on the idea of controlled chemical release via particle technology described in previous chapters, we devised a plan to develop a chemical display system that would be able to address some of the limitations found from electronic display. The concept of a chemical display would benefit from the absence of components or interfaces that connect each pixel, allowing increased freedom in both design and utility. For example, a chemical display system could be built onto a variety of substrates including hard and flexible substrates in both 2D and 3D. We aim to construct the system based on an array of self-assembled micropolyhedra, a structure that can be produced in a very efficient and parallel manner. Detailed

information about surface tension driven self-assembled polyhedra is described in previous chapters.

We first note our past research work involving self-assembled micropolyhedra to enable controlled chemical release. In 2006, Leong et.al developed a 3D metallic micro containers with controlled surface porosity that enables a pico-nanoliter scale chemical encapsulation and delivery [54]. However, the previous work only consisted of a simple demonstration of the controlled dye release from a container (**Figure 19**).
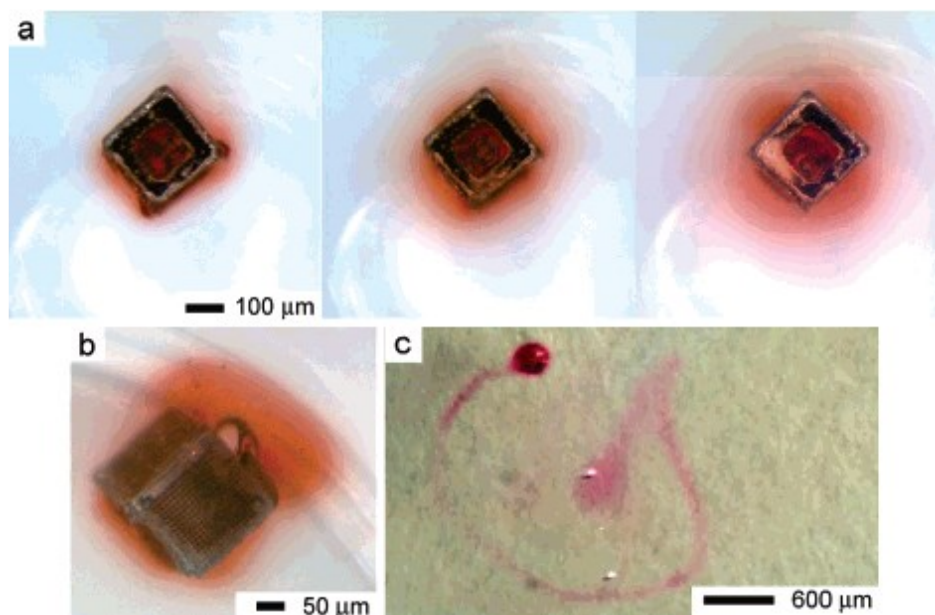
Figure 19. Optical images of chemical release from microscale porous cube. (a) Spatially isotropic release of a dye from a container with identical porosity on all faces. (b) Anisotropic release of a dye from a container with anisotropic porosity (five faces with an array of 5 micron pores; the sixth face has a 160 micron sized pore). (c) An example of a remotely guided spatially controlled chemical reaction. Reprinted with permission from [54]. © 2007 American Chemical Society.

Based on the highly versatile and tunable particle technology ideal for enabling controlled chemistry, we herein describe a concept of a chemical display system that can generate a set of moving visual images by the unprecedented 3D spatial control of chemical release. We plan to construct the chemical display system by creating an array of precisely engineered self-folded metallic porous cubes with

various tunable properties such as dimensions, pore sizes, chemical concentrations and arrangements loaded with dyes to be released.

With electronic display's exceptional performance and extensive list of advantages already in place, our goal is not to replace electronic display. Instead, we anticipate that advantages of the chemical display would be able to complement existing display systems by providing new capabilities for dynamic display technology in multiple applications. We view several advantages in our chemical display system: (1) a back-end interface free system without the need for external power sources, (2) a wide range of substrates onto which the chemical display can be installed and (3) a highly versatile and tunable porous cube that allows the adjustment of the produced image.

3.2 Key design considerations and approach

3.2.1 Means of enabling a controlled chemical release

Past studies reveal that there are various ways of enabling controlled chemical release. The possible means of enabling controlled chemical release in continuous or discontinuous form include: (1) a diffusion that allows the spontaneous release of chemicals and (2) external stimuli such as temperature, pH level, ultrasound, electric current and magnetic field that allow the release of chemicals in response to stimuli. [55-60].

We chose to utilize diffusion for the spontaneous controlled chemical release for our experiment in order to maximize the utility of our chemical display system based on its tunability and ease of use. The use of external stimuli would be possible, but it would limit the utility of the chemical display system due to their complicated and costly process.

3.2.2 Concept of chemical voxels

Similar to individual pixels found in electronic display, we utilize precisely patterned and chemically loaded 3D porous metallic cubes fabricated by surface tension driven self-assembly and refer them as chemical voxels. Although different types of containers that are well-developed such as porous capsules and microgel particles can be used as chemical voxels, controlling the chemical release from these types of containers is highly difficult [61,62]. Also since the porous metallic cubes can withstand prolonged use thanks to its robust structure, they are better suited for chemical displays. **Figure 20** illustrates different types of containers that can be utilized as chemical voxels.
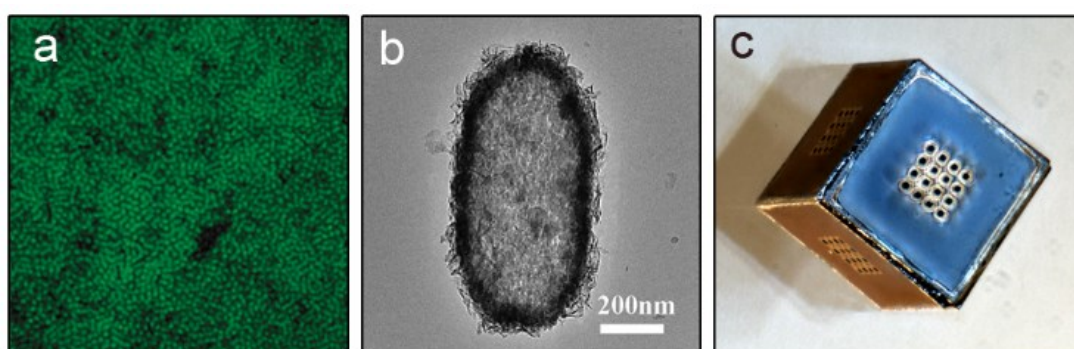
Figure 20. Different types of containers that can be utilized as chemical voxels. (a) Fluorescence microscopic images of three-layer FITC insulin microgel thin film for thermally modulated insulin release. Reprinted with permission from [61]. © 2004 American Chemical Society. (b) SEM image of Hydroxyapatite nanostructured hollow ellipsoidal capsules for application in drug delivery. Reprinted with permission from [62]. © 2008 Royal Society of Chemistry. (c) Optical image of microscale porous metallic cube fabricated by surface tension driven self-assembly.

Through the fine tuning of different characteristics of chemical voxels placed in arrays, such as the concentration of chemical and controlled release time of chemicals, we would obtain dynamic visual images via spatial and temporal control of chemical release.

3.2.3 Demonstrating the concept of a chemical display

To demonstrate the concept of a chemical display, we will first conduct multiple numerical simulations followed by a series of experiments and show how the variations in multiple designing parameters such as the concentration of chemicals, porosity, volume, shape and the positioning of the chemical voxels can be utilized in order to control the dynamics of the produced image from our chemical display system. Then we will provide a proof-of-principle by demonstrating an animation of a running man produced from an array of chemical voxels via controlled chemical release. Finally, we conclude by addressing the compatibility of a chemical display system to be implemented onto various substrates including both rigid and flexible substrates.

To sum up, the three key principles of our chemical display system is as follows: (1) a high throughput strategy to synthesize chemical voxels with adjustable characteristics such as volume, shape and porosity, (2) design criterion for programmed chemical release with both local and global control based on numerical simulations and (3) a strategy to dispense and arrange the voxels into well-ordered arrays onto multiple types of substrates.

3.3 Experimental methods

3.3.1 Numerical simulations of a controlled chemical release from voxels

All of the numerical simulations in this study was performed using COMSOL Multiphysics (COMSOL, Inc.). In our simulations, we assumed that the voxels were surrounded by a 4 mm thick stationary medium and sought solutions to the time-dependent diffusion equation in stationary medium in the absence of chemical reactions as described previously [63,64].

26

Prior to conducting the final round of simulations for the exact types of chemical voxels that we would use to construct our arrays for the chemical display, we first conducted simulations to find the chemical concentration variation as a function of distance away from a voxel by working with two types of chemical voxels: 500 μm cube with a single 100 μm pore on each face and 250 μm cube with a single 3μm pore on each face. The simulation result is shown below in **Figure 21**.
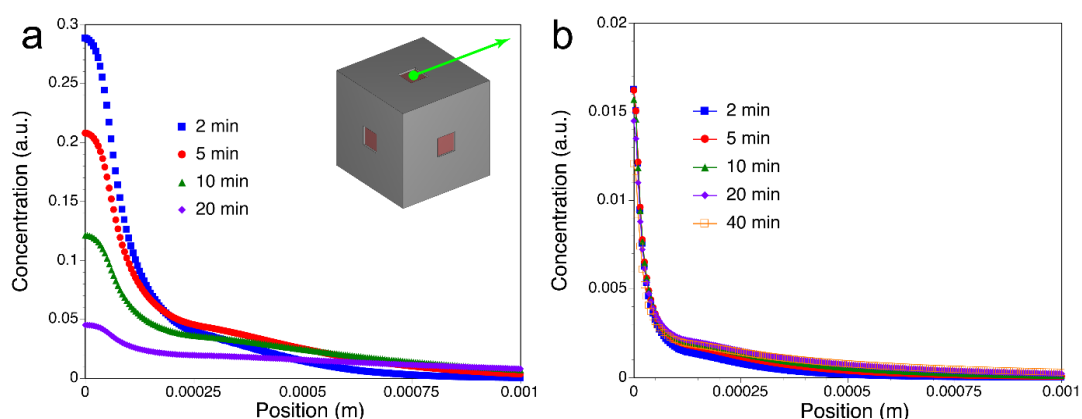
Figure 21. Simulation results showing the concentration variation as a function of distance away from a voxel plotted along the line shown in green in the inset for different times. The voxel used for simulation is a 500 μm cube with a single 100 μm pore on each face for (a) and a 250 μm cube with a single 3 μm pore on each face for (b). Reprinted.

Based on this simulation result, we then conducted different sets of simulations in order to demonstrate the temporal control over the chemical release from chemical voxels with varying design parameters. This result is shown in **Figure 22** in the results section.

Our final round of simulation was on dynamic visual images of that would be produced from our chemical display system. We conducted the simulation using three types of chemical voxels as described in **Table 1**. The simulation results were obtained by plotting the concentration field in a plane parallel to the plane of the voxels and by offsetting from it by 600 μm. Photobleaching of the fluorescent dye was not taken into

account in the simulations. In addition, when simulating the chemical release from individual voxels we assumed zero boundary conditions thus neglecting possible chemical interactions between voxels. Such interactions were taken into account in simulations of the chemical release from ordered voxel arrangements.

3.3.2 Fabrication of chemical voxels

In this study, all of the chemical voxels were fabricated using the surface tension driven self-assembly technique in which patterned 2D templates get folded into 3D structures due to minimization of surface energy of the molten hinges. Detailed information of this technique is listed in previous chapters.

We designed planar templates of voxels based on the design rules described in previous chapters using AutoCAD and printed them on transparency film to make photomasks. We utilized these photomasks for photolithography processes including the patterning of 2D panels and hinges, followed by electroplating and wet etching. In order to release the 2D templates of the chemical voxels, we used etchants APS100 and CRE-473 to dissolve the sacrificial layer. Then we heated the released templates to 100°C, with the addition of liquid flux. Then we slowly increased the temperature to 150°C, then finally to 200°C until the voxels were folded completely. [47].

3.3.3 Experimental setup of the chemical display system

For the animation of a running man, we positioned three different types of cubic voxels manually to form three frames of a running man figure and attached them on glass slides using an adhesive (Gorilla Glue; Catalog No. 23629-1002). In order to facilitate the chemical display, we loaded the arrayed voxels with fluorescein (Sigma-Aldrich; Fluorescein Sodium Salt, Catalog No. 231-791-2) by soaking them in aqueous solutions overnight. In the case of voxels with small pores, the voxels were placed in a

desiccator to remove air bubbles and speed up the loading process. The concentrations of chemicals loaded in the voxels were calculated in accordance with the numerical simulations. **Figure 22** shows the schematic diagram of the experimental set up and **Table 1** describes the experimental setup of chemical voxels used to generate a dynamic image of a running man.
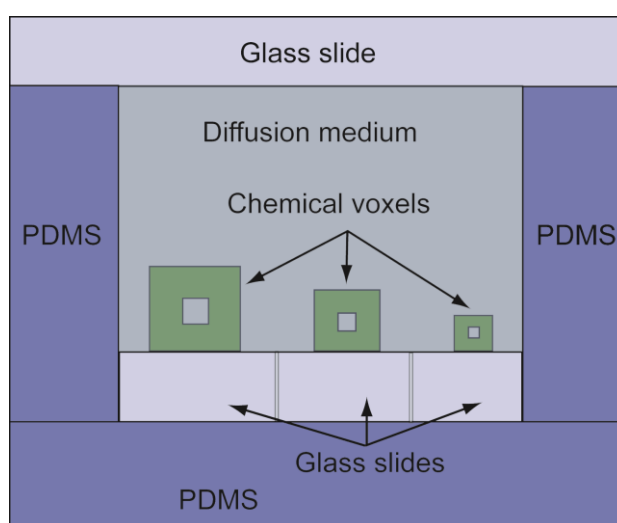
Figure 22. Schematic diagram of the experimental setup of the chemical display system. The voxel used for simulation is a 500 μm cube with a single 100 μm pore on each face for (a) and a 250 μm cube with a single 3 μm pore on each face for (b). Reprinted.

Table 1. Experimental setup of chemical voxels for the chemical display system.

Frame #	Size of each voxel	Pore size and type	Number of voxels	Fluorescein concentration
a	500 μm	25 μm pores, 4x4 array	19	2 mM
b	400 μm	17 μm, single pore	26	4 mM
c	250 μm	3 μm, single pore	36	15 mM

3.3.4 Implementing the chemical display system onto substrates

For the implementation of the chemical display system onto a substrate, the chemical voxels can either be positioned manually or by nozzle based printing methods. In order to set up our chemical display system in a house shape shown in **Figure 27**,

we added approximately 200 cube shaped voxels in a 2 mL (1% w/v) agarose gel and mixed them well using a pipette. We used a disposable transfer pipette (Fisherbrand™; Catalog No. 13-711-7M) to dispense the voxels and write a shape of house on a glass slide. The gel solidified in 5-7 minutes at room temperature.

To create the design of a man on a flexible surface shown in **Figure 27**, we first mixed the elastomer base and curing agent (Dow Corning Sylgard® 184 Silicone Elastomer Kit) in a ratio of 10:1 (w/w) and put it in a desiccator to remove bubbles. After removing the bubbles, we cured it at 65°C for 2 hours to prepare a flexible polydimethylsiloxane (PDMS) substrate. Then, 300 μm sized dodecahedron shaped voxels were positioned manually on the PDMS substrate and attached with an adhesive (Gorilla Glue; Catalog No. 23629-1002). We loaded these voxels by covering them with a green color liquid dye (McCormick Food Color & Egg Dye) and placing the substrate in a desiccator for 10 minutes to speed up the loading process. We removed the excess dye by rinsing the voxels with distilled water and dried the excess by wiping with KimWipes™.

3.3.5 Chemical diffusion and imaging

In order to generate the moving images of the running man shown in Figure 25, we rinsed loaded chemical voxels briefly with water and gently wiped them to remove any excess fluorescein that remained on the outer surface of the voxels. Then we placed the arrayed voxels in a 4 mm tall PDMS chamber and activated the display by gently pouring a mix of glycerol, ethyl alcohol and water in a ratio of 2:1:1 (v/v) onto the chemical voxels. Once diffusion began, we imaged the diffusion of fluorescein under a fluorescence microscope. Each frame was imaged separately but at the same time and then stitched together to make an animation of three frames thus illustrating a running

man figure from left to right. The voxels were used and reused for image formation over 10 times.

3.4 Results and discussions

3.4.1 Simulations of the controlled chemical release from voxels

In order to demonstrate the controlled chemical release from chemical voxels via the fine tuning of various designing parameters, we investigated the controlled chemical release from a self-assembled cube with porous walls as shown in **Figure 23a**.

When the porous cubic voxel filled with a chemical is placed into a stationary diffusion medium, the spontaneous diffusion the chemical occurs through the pores on the surface. This means that we can control the temporal characteristics of the chemical release, such as its duration of release, timings of start and peak of the chemical diffusion process by manipulating geometric design parameters such as porosity, shape and volume of the voxels.

In order to simulate the controlled chemical diffusion from chemical voxels, we had to define two key terms in regards to the chemical diffusion. Firstly, we defined the "start" of the chemical release as the time when chemical starts coming out and its concentration in the vicinity of the voxel is one half (1/2) of the maximal value. Then we defined the "peak" as the time when the concentration in the vicinity is maximal and the "end" as the time when the concentration of the chemical reaches one half (1/2) of its maximal value in the vicinity of the voxel.

Based on the spatial profile of the chemical concentration around a cubic voxel in a stationary diffusion medium shown in **Figure 21**, we simulated how the manipulation of geometric design parameters of a chemical voxel would affect the temporal

characteristics of the chemical release, such as its duration of release, timings of start and peak of the chemical diffusion. The simulation results shown in **Figure 23b** suggest that the separation of starts and peaks can be controlled by varying the pore sizes and dimensions of voxels. For example, smaller pores would result in a slower release of chemicals from the pores of the chemical voxel, causing the duration of a chemical release to increase.
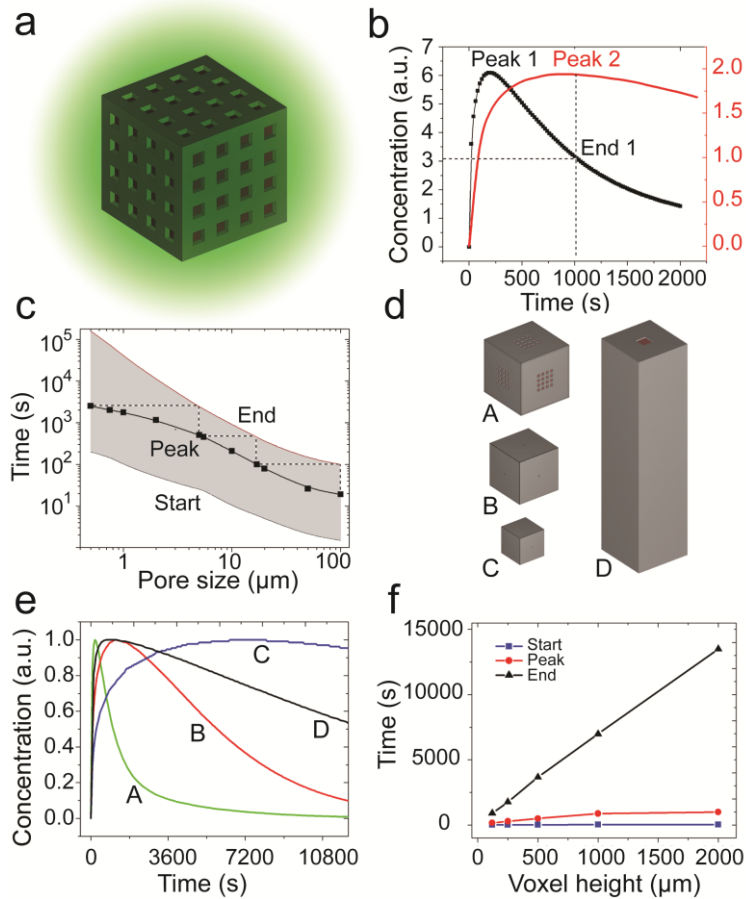
Figure 23. Numerical simulation results of the controlled chemical release from chemical voxels. Numerical simulation results demonstrating temporal control over chemical release from chemical voxels with different shapes, sizes and pore characteristics. (a) Schematic illustration of chemical diffusion from a cubic voxel. (b) The variation of chemical concentration diffused from the voxel as a function of time. Black line corresponds to diffusion from a 500 μm size cubic voxel with a single 100 μm pore on each face, and red line corresponds to a 500 μm size cubic chemical voxel with a single 20 μm size pore on each face. (c) Plot of the time of chemical release as a function of pore size. The start, peak and end points of chemical release are plotted for a 500 μm size cubic chemical voxel. The dashed lines in the plot illustrate the procedure for synchronizing release times from voxels with different pore sizes. For example, in this plot, when the chemical release from a voxel with 100 μm size pore ends, the release from a voxel with 20 μm size pore reaches the peak. This way we can engineer these chemical voxels when a given voxel would become visible and when it would fade away. (d) Images of voxels with various time release characteristics. (A-C) are chemical voxels described in Table 1 and (D) is a parallel pipe with dimensions 2000 μm by 500 μm by 500 μm with a single 100 μm pore. (e) Numerical simulation plot of chemical concentration as a function of time for the voxels shown in (d). (f) Time of chemical release plotted as a function of voxel volume. Voxels have same pores and cross-section (500 μm x 500 μm) with varying heights. It shows that we can control the duration of chemical release by using voxels with different volumes. Reprinted.

Our simulation results shown above indicates that it is possible for us to precisely "engineer" the chemical voxels to generate a dynamic image synchronizing the release times from different chemical voxels via a fine tuning of geometric design parameters such as the pore size and volume of the voxels. For example, some voxels will only

start releasing chemicals when other voxels have released almost all of their content. This approach can be utilized for "programming" various time-dependent chemical patterns by placing precisely designed voxels in the immediate vicinity of each other. Since the duration of the chemical release depends on pore size and volume of the voxel, we can use voxels of different geometry with different pore characteristics to control the separation of peaks and the duration of chemical release as illustrated in simulation results shown in **Figure 23** above.

3.4.2 Designing the chemical display system

In this study, we demonstrate the concept of a chemical display by arranging chemical voxels with different geometric design parameters in an array to generate dynamic images of a running man. In order to do so, we first visualized the dynamic image first by simulation. As in conventional animations, we broke up the moving image of the running man into a sequence of three static images and performed numerical simulations in order for us to be able to "engineer" the chemical voxels with different volumes, pore sizes and chemical concentrations into appropriate arrangements to produce our desired image. The dynamic image that we can our chemical display system to generate was made available via numerical simulations and is shown below in **Figure 24**.
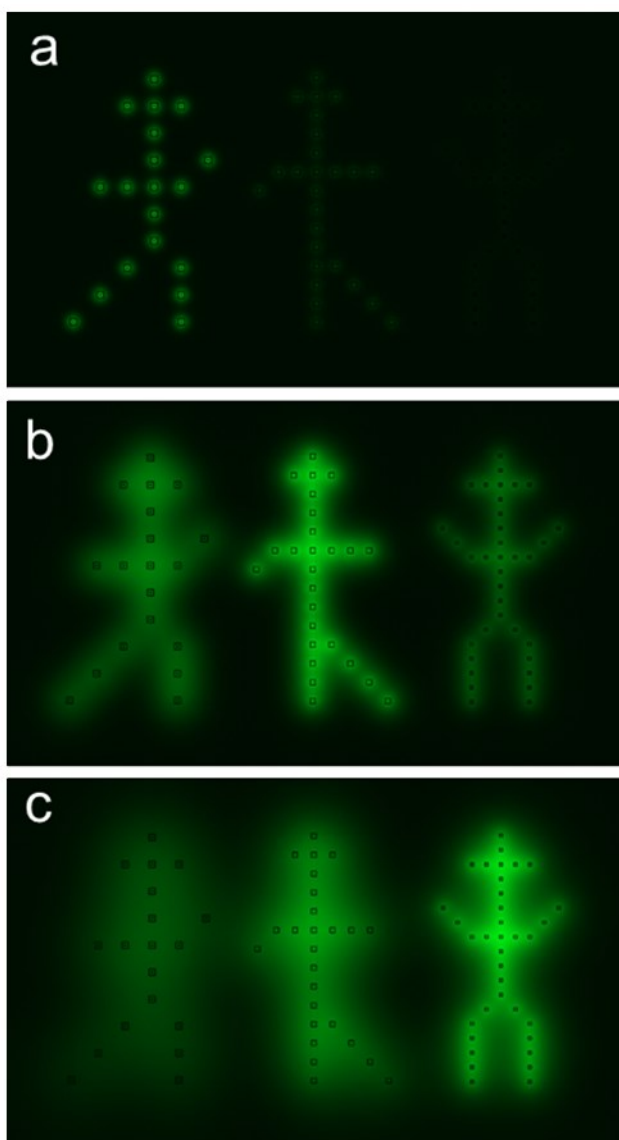
Figure 24. Simulation results of the chemical display system showing dynamic images of a running man. (a-c) Sequential generation of dynamic images of a running man from left to right. The geometric design parameters of the chemical voxels used in the simulation are listed in Table 1. Reprinted.

In order to control the release time of chemicals diffusing out from different arrays, the voxel volume and pore size were varied in simulation. Our simulation result above suggests that a dynamic image shown above (from left to right) can be generated by arranging chemical voxels with decreasing volume, decreasing pore size and increasing concentration from left to right. In order to engineer our chemical display system to generate the dynamic image shown in the simulation, we would have to construct the frame on the left with voxels of the largest volume, largest pore size and lowest

chemical concentration while we would construct the frame on the right the with voxels of the smallest volume, smallest pore size and highest chemical concentration and so forth. This process would ensure the duration of chemical release for each image frames to be well separated thereby producing a set of dynamic images where the concentration of chemicals from diffusion is precisely controlled.

As shown above, our simulations suggest that dynamic images can be generated by carefully engineering each frames with an arrangement of appropriately designed voxels with varying geometric design parameters and the concentrations of loaded chemicals. To create a single animation, the frames can be arranged either in the same location or on top of each other.

3.4.3 Experimental validation of the chemical display and implementation of the chemical display onto multiple substrates

In order to validate our concept of a chemical display experimentally, we built our chemical display system by attaching three different types of fluorescein-loaded cubic voxels onto glass substrates.

The chemical voxels we utilized in our chemical display were fabricated by surface tension driven assembly, a process that has been detailed in previous chapters. By using well-known lithography steps and microfabrication steps detailed in the experimental methods section above, we first fabricated three groups of cubic voxels with different geometric design parameters. The properties of three different types of chemical voxels with varying properties are shown in **Table 1**. Then we arranged them in multiple arrays on a glass slide to represent chemical voxels for the generation of three distinct frames of a running man in the chemical display. The optical image of the experimental setup of the chemical display is illustrated in **Figure 25** below.

36
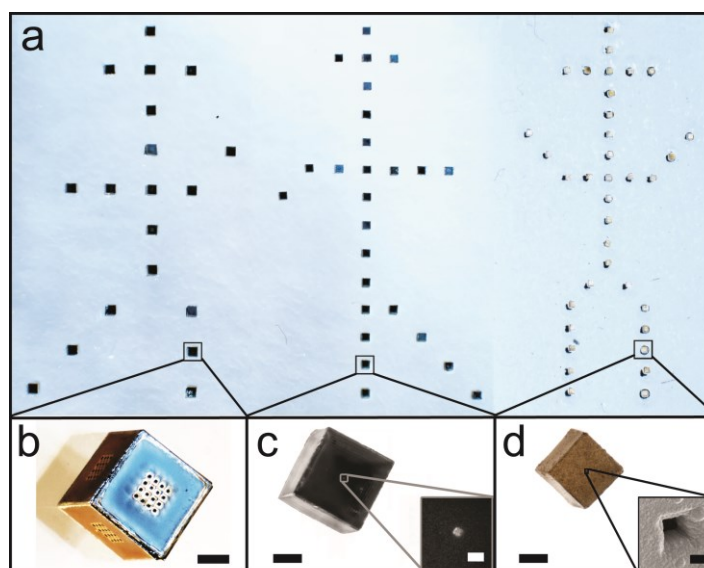
Figure 25. Optical image of the experimental setup of the chemical display. (a) Top view of the chemical voxels arranged on a glass slide that represent the first, second and third frames of a running man. (b-d) The three different types of chemical voxels used in the chemical display. Detailed information is listed in Table 1. The inset in (c) is a zoomed image of a 17 μm size pore and the inset in (d) is a zoomed SEM image of a 3 μm size pore. Scale bars are 100 μm for (b), (c), (d), 30 μm for the inset in (c) and 2 µm for the inset in (d). Reprinted.

After setting up the chemical display, we loaded each voxels with fluorescein to visualize the image shown in our simulation. Instead of fluorescein, different dyes or chemicals could also be utilized. To trigger the image generation, we gently poured our diffusion medium. As we hypothesized, the first frame appeared at the time when the fluorescence intensity of fluorescein released from the chemical voxels constituting this frame reached its peak. When the fluorescence intensity of the first frame was decreased to the half of its maximal value, the fluorescence intensity of the voxels in second frame reached the peak and thus the second frame became visible. Similarly, when the fluorescence intensity of the chemical voxels in the second frame was reduced to half of its maximal value, the third frame became visible. Hence, the three frames appear one after the other from left to right in agreement with simulations, thereby validating our concept of a chemical display. **Figure 26** shows this experimental validation of our chemical display.
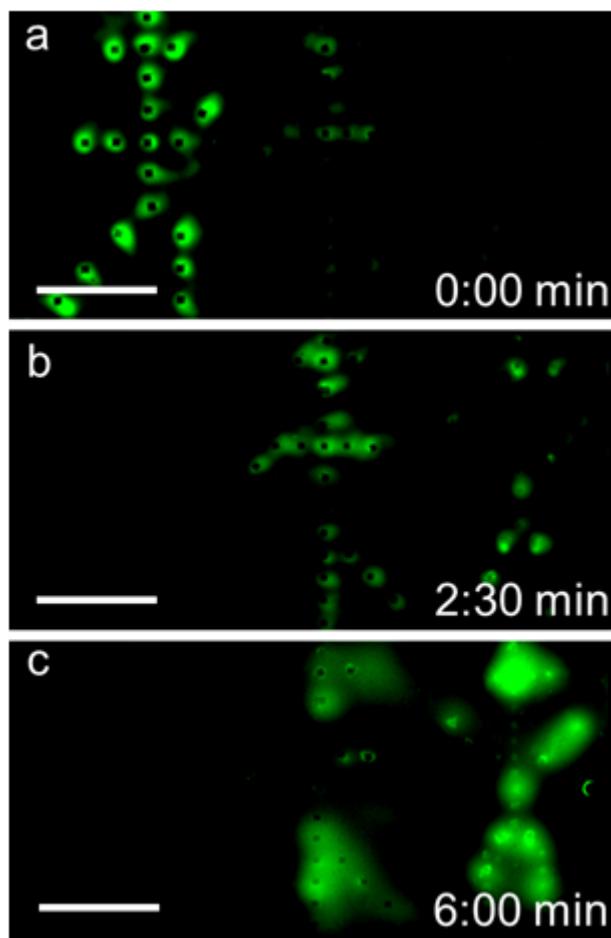
Figure 26. Experimental demonstration of the chemical display. Experimental demonstration of the chemical display depicting a man running from left to right. (a-c) Experimental results showing time dependent images of the frames of a running man via fluorescein diffusion from chemical voxels in a diffusion medium consisting of glycerol, ethanol and water in a ratio of 2:1:1. All three frames were imaged separately at the same time and then the frames were stitched together. (a) Initially only the first frame becomes visible. (b) After 2:30 min, the first frame completely fades away and the second frame becomes visible. (c) Finally at time 6:00 min, the first two frames fade away and the third frame becomes visible. Scale bars: 1 cm. Reprinted.

After the experimental validation of the chemical display, we also show that the voxels can be implemented onto different substrates with to highlight the use of our methodology with conventional artistic media. By using a voxel-loaded pipette, we were able to write the shape of a house as shown in **Figure 27** below.
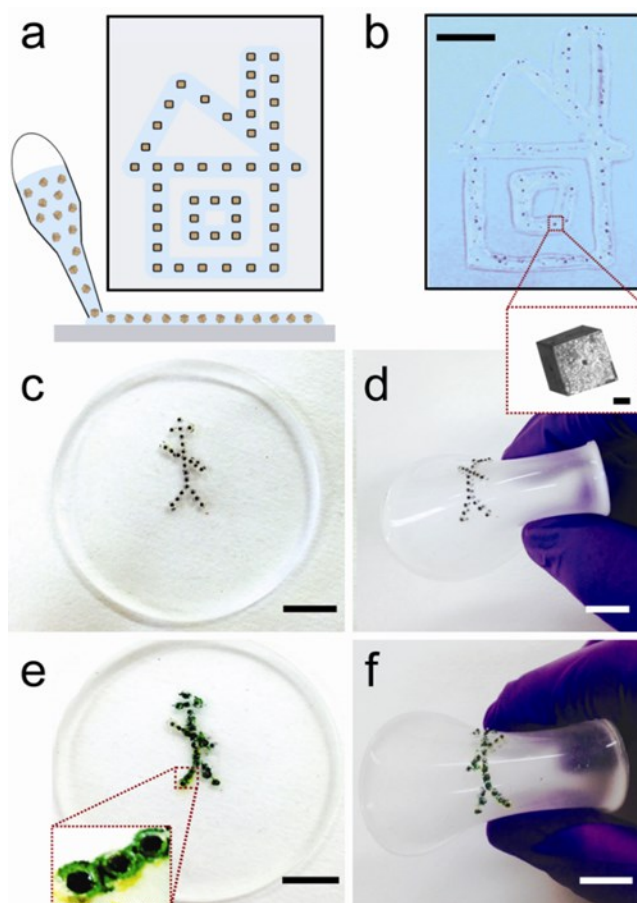
Figure 27. Demonstration of implementation of the chemical display on rigid and flexible surfaces. (a) Schematic illustration of the dispensation of chemical voxels using a nozzle-based approach to create the shape of a house on a glass slide. (b) Optical image depicting voxels written using pipette filled with agarose gel in the shape of a house. The agarose gel serves as a diffusion medium to visualize chemicals released from the voxels. The zoomed inset is an optical image of a single cube shaped chemical voxel. (c, d) Optical images of dodecahedron-shaped chemical voxels arranged on a polydimethylsiloxane (PDMS) surface to illustrate an artistic design of a man on a flexible substrate. (e, f) Optical images showing chemical diffusion from dye loaded chemical voxels on the PDMS surface. Scale bars: 1 cm for (b-f) and 100 μm for the inset in (b). Reprinted.

Although we wrote the shape of a house with chemical voxels by hand, we believe more efficient computer controlled nozzle-based printing techniques can be utilized to implement chemical displays onto various substrates in both 2D and 3D [69,70]. **Figure 27** above demonstrates that chemical voxels can be arranged on a variety of substrates including both on rigid and flexible substrates.

3.4.4 Fundamental limitations of the chemical display and potential issues

Although we have successfully demonstrated the concept of a chemical display with a proof-of-principle, it is critical that we note some of the fundamental limitations and drawbacks of chemical displays described in this study. While a concept of a chemical display would benefit from the absence of components or interfaces that connect each pixel, allowing increased freedom in both design and utility, there are fundamental limitations that are inherent to chemical displays due to its operating mechanism.

Firstly, the concept of a chemical display demonstrated here is non-reversible due to its working mechanism in which the information to be displayed is geometrically encoded within individual chemical voxels to generate a certain image. Once an image is generated, it gradually diffuses away over time and the chemical display system is unable to display any information until the system is re-loaded with the chemicals required to operate the display. Our current design of a chemical display lacks the repeatability or reversibility, a factor that is often critical to display technology and it will have to be addressed this issue in the future.

In addition, we may also need to revise the current means of activation of our display described here. Because we built the chemical display system with voxels loaded with chemicals, there is a possibility that the chemicals may begin to diffuse immediately after the fabrication of the display even before the addition of diffusion medium. Also, since our current work only demonstrates a spontaneous release of chemicals upon the addition of diffusion medium, we plan to develop a different way to control the activation of the display in the upcoming research. This can include activating chemical voxels with external stimuli such as light, laser and radio frequency allowing on-demand or remotely controlled display [55-60].

Other issues to be addressed in future studies include the environmental and sustainable aspects of the display, such as handling, storage and disposal of chemicals.

3.4.5 Applications of a chemical display

Our results above shows a proof-of-concept for the fabrication and the demonstration of a fully functional chemical display. As we emphasized above, while we do not expect our chemical displays to be able to match the robust performance of electronic displays including rapid frame rates and response time at the current stage of development, we believe that chemical displays can serve a unique role in media applications. Benefitting from its back-end interface free system without a need for external power sources and a wide range of 2D and 3D substrates onto which the chemical displays can be installed, chemical displays can serve as a relatively simple and compact display system such as greeting cards with animations, animated signs and more. In future studies, by developing a chemical display with an advanced design where voxels are precisely arranged on a pre-existing grid with a high resolution (higher number of voxels in a given area) based on traditional ink-jet or 3D printing technologies, more complex and dynamic images can be generated [69,70].

In addition to media applications, we also envision that spatially controlled chemical pattern formation from chemical voxels can offer a broad range of other applications such as controlled drug delivery in micro and nanoscale, chemical kinetics and reaction diffusion system. For example, In addition to media applications, we envision that the methodology could also be used in biotechnology and bioengineering to create programmable chemical patterns such as dynamic gradients to direct cellular behaviors [63,64]. This methodology would complement existing techniques, while allowing for precisely controlled release of chemicals by relying on the different geometric design parameters of the voxels such as shape and size.

CHAPTER 4. FUTURE OUTLOOK AND CONCLUSIONS

4.1 Future outlook

As briefly mentioned in the previous section, one of the biggest issue our current design of a chemical display is the non-reversibility. In our future studies, we believe that we may be able to address this issue by designing a chemical display based on reversible chemical reactions instead of a controlled chemical diffusion of non-reactive chemicals.

An excellent example of such chemical reaction is the Belousov-Zhabotinsky (BZ) reaction, an interesting chemical reaction that results in a nonlinear chemical oscillator in which the color of the reaction mixture oscillates between red and blue due to multiple cycles of oxidation and reduction reactions of chemicals involved. **Figure 28** below gives an overview of the BZ reaction.

$$BrO_3^- + Br^- + 2\,H^+ = HBrO_2 + HOBr \qquad (A1)$$
$$HBrO_2 + Br^- + H^+ = 2HOBr \qquad (A2)$$
$$HOBr + Br^- + H^+ = Br_2 + H_2O \qquad (A3)$$
$$BrO_3^- + HBrO_2 + H^+ = 2BrO_2{\cdot} + H_2O \qquad (B1)$$
$$BrO_2{\cdot} + Fe(II) + H^+ = HBrO_2 + Fe(III) \qquad (B2)$$
$$2HBrO_2 = BrO_3^- + HOBr + H^+ \qquad (B3)$$
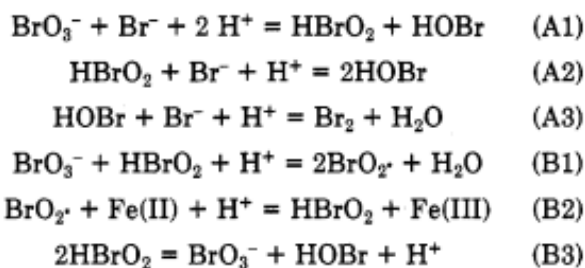
Figure 28. An overview of oxidation reaction of Acidic Bromate responsible for color change in the BZ Reaction. Reprinted with permission from [68]. © 1981 American Chemical Society.

Our lab has also worked with the BZ reaction extensively with some interesting results. **Figure 29 to 32** illustrates some of our findings on the BZ wave propagation in systems with different geometries and boundary conditions.
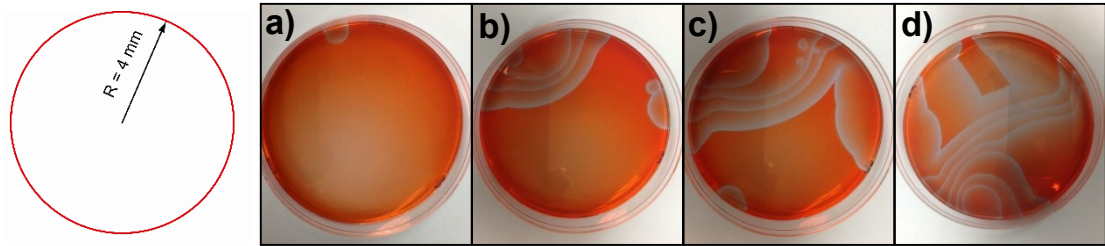
Figure 29. BZ wave propagation in a circular petri dish of radius 4 mm.
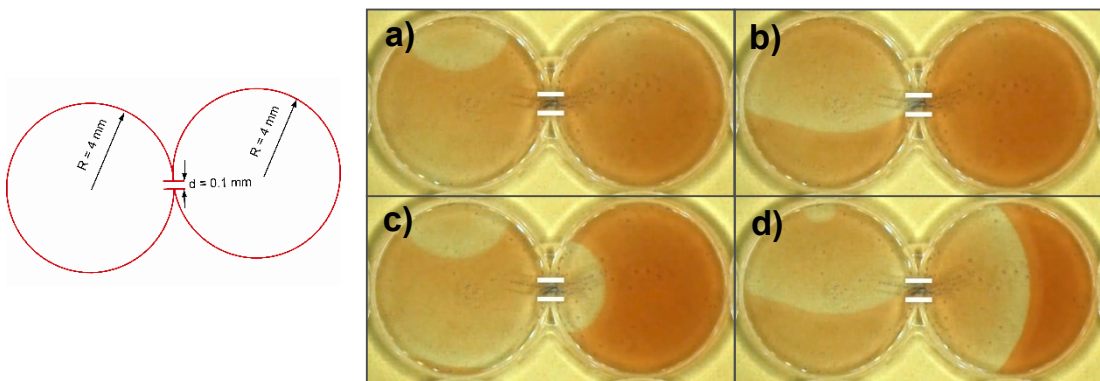
Figure 30. BZ wave propagation from one circular geometry to another circular geometry (radius = 4 mm) through a narrow opening (d = 0.1 mm).
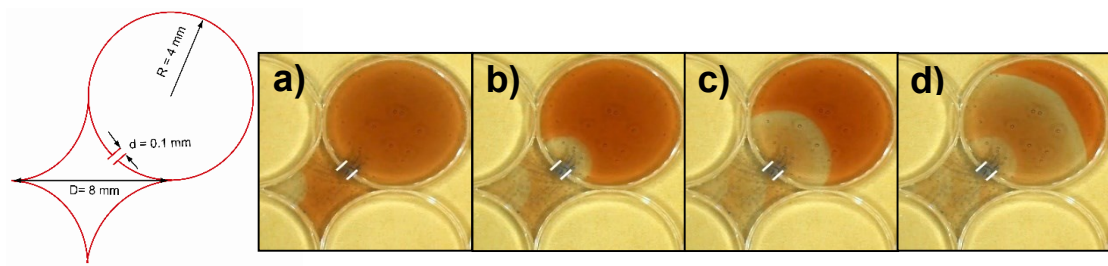
Figure 31. BZ wave propagation from a diamond geometry to a circular geometry through a narrow opening (d = 0.1 mm).

Figure 32. BZ wave propagation along a narrow channel of diameter 0.5mm.

Due to a drastic color change and reversibility, we believe that the BZ reaction may hold some value in chemical displays and may provide us some clue in addressing the issue of reversibility in chemical displays. In addition to the BZ reaction which is produces a chemical oscillator, there are also other reversible chemical reactions with color change that may be useful in chemical displays, such as the chemical reaction between ammonia and phenolphthalein or copper sulfate.

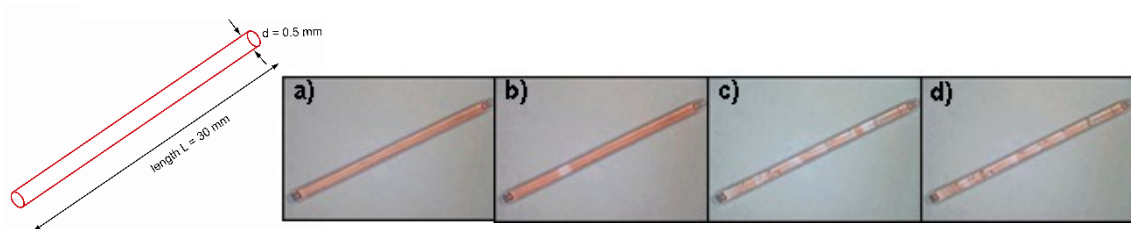In future studies, we plan to build an improved chemical display system with reversible chemical reactions that produce a distinct color change in the hopes of resolving reversibility. In addition, we can also implement a source and sink system in order to address current issues with the controlled activation of display.

4.2 Conclusion

In this thesis, we have reviewed the importance of spatially controlled chemistry via particle technologies and the surface tension driven self-assembly technique to mass produce various polyhedra, one of the most attractive model system that has broad implications in multiple fields of study.

Using self-assembled porous cubes in microscale, we have successfully demonstrated the fabrication and operation of a chemical display based on three key principles of (a) a high throughput strategy to synthesize chemical voxels with adjustable characteristics such as volume, shape and porosity, (b) design criterion for programmed chemical release with both local and global control based on numerical simulations and (c) a strategy to dispense and arrange the voxels into well-ordered arrays in multiple types of substrates.

Thanks to its design with the absence of components or interfaces that connect each pixel, we expect chemical displays to offer increased freedom in both design and utility

and complement existing display systems, opening up new possibilities in other fields of study such as biotechnology, chemistry and bioengineering benefitting from a sequential release of chemicals, cells and more.

While we note several drawbacks and limitations from our chemical display such as non-reversibility and uncontrolled spontaneous activation of chemical voxels, we plan to address them by utilizing reversible chemical reactions with source and sink system in our future studies.

REFERENCES

[1]   Kalinin, Y. V.; Murali, A.; Gracias, D. H. Chemistry with spatial control using particles and streams. *RSC Adv.* **2012**, *2*, 9707-9726.

[2] Rosch, J.; Caparon, M. A Microdomain for Protein Secretion in Gram-PositiveBacteria. *Science* **2004**, *304*, 1513-1515.

[3] Shapiro, L.; McAdams, H. H.; Losick, R. Why and How Bacteria Localize Proteins. *Science* **2009**, *326*, 1225-1228.

[4] Goley, E. D.; Iniesta, A. A.; Shapiro, L. Cell cycle regulation in Caulobacter: location, location, location. *Journal of Cell Science* **2007**, *120*, 3501-3507.

[5] Scott, M. E.; Dossani, Z. Y.; Sandkvist, M. Directed polar secretion of protease from single cells of Vibrio cholerae via the type II secretion pathway. *Proceedings of the National Academy of Sciences* **2001**, *98*, 13978-13983.

[6]   Atiyah, M.; Sutcliffe, P. Polyhedra in Physics, Chemistry and Geometry. Milan *Journal of Mathematics* **2003**, 71, 33-58.

[7]   Torquato, S.; Jiao, Y. Dense packings of polyhedra: Platonic and Archimedean solids. *Phys. Rev E.* **2009**, 80, 041104.

[8]   Cromwell, P. R. Polyhedra; Cambridge University Press: Cambridge, U.K.; New York, **1997**; pp 451.

[9]   Pugh, A. Polyhedra : a visual approach; The Dome series; University of California Press: Berkeley, **1976**; , pp 118.

[10]   Zandi, R.; Reguera, D.; Bruinsma, R. F.; Gelbart, W. M.; Rudnick, J. Origin of icosahedral symmetry in viruses. *Proceedings of the National Academy of Sciences of the United States of America* **2004**, 101, 15556-15560.

[11]   Lazar, E. A.; Mason, J. K.; MacPherson, R. D.; Srolovitz, D. J. Complete Topology of Cells, Grains, and Bubbles in Three-Dimensional Microstructures. *Phys. Rev. Lett.* **2012***, 109*, 095505.

[12]   Senechal, M. Shaping Space: Exploring Polyhedra in Nature, Art, and the Geometrical Imagination; Springer New York: **2013**;.

[13]   Bishop, R. H. *Mechatronic systems, sensors, and actuators: fundamentals and modeling;* Taylor & Francis: Boca Raton, **2008**..

[14]   Pandey, S.; Gultepe, E.; Gracias, D. H. Origami Inspired Self-assembly of Patterned and Reconfigurable Particles. *Journal of Visualized Experiments: JoVE* **2013**, 50022.

[15]   Bustillo, J. M.; Howe, R. T.; Muller, R. S. Surface micromachining for microelectromechanical systems. *Proc IEEE* **1998***, 86*, 1552-1574.

[16]   Gracias, D. H.; Kavthekar, V.; Love, J. C.; Paul, K. E.; Whitesides, G. M. Fabrication of Micrometer-Scale, Patterned Polyhedra by Self-Assembly. *Adv Mater* **2002***, 14*, 235-238.

[17]   Eun Sok Kim. Piezoelectric MEMS for audio signal transduction, microfluidic management, resonant mass sensing, and movable surface micromachined structures*;* Ultrasonics Symposium, 2008. IUS 2008. *IEEE*; 2008; , pp 924-929.

[18]   Xia, Y.; Whitesides, G. M. Soft Lithography. *Angewandte Chemie International Edition* **1998***, 37*, 550-575.

[19]   Piotter, V.; Hanemann, T.; Ruprecht, R.; Hausselt, J. Injection molding and related techniques for fabrication of microstructures. *Microsystem Technologies* **1997***, 3*, 129-133.

[20]   Kimerling, T.; Liu, W.; Kim, B.; Yao, D. Rapid hot embossing of polymer microfeatures. *Microsystem Technologies* **2006**, *12*, 730-735.

[21]   Xia, Y.; McClelland, J. J.; Gupta, R.; Qin, D.; Zhao, X.; Sohn, L. L.; Celotta, R. J.; Whitesides, G. M. Replica molding using polymeric materials: A practical step toward nanomanufacturing. *Adv Mater* **1997**, *9*, 147-149.

[22]   Wang, J.; Chen, Q. Microfabricated phenol biosensors based on screen printing of tyrosinase containing carbon ink. *Anal. Lett.* **1995**, *28*, 1131-1142.

[23]   Whitesides, G. M.; Boncheva, M. Beyond molecules: self-assembly of mesoscopic and macroscopic components. *Proc. Natl. Acad. Sci. U. S. A.* **2002**, *99*, 4769-4774.

[24]   Mendes, A. C.; Baran, E. T.; Reis, R. L.; Azevedo, H. S. Self-assembly in nature: using the principles of nature to create complex nanobiomaterials. *Wiley Interdisciplinary Reviews: Nanomedicine and Nanobiotechnology* **2013**, *5*, 582-612.

[25]   Whitesides, G. What Will Chemistry Do in the Next Twenty Years? *Angewandte Chemie International Edition in English* **1990**, *29*, 1209-1218.

[26]   Bowden, N.; Terfort, A.; Carbeck, J.; Whitesides, G. M. Self-Assembly of Mesoscale Objects into Ordered Two-Dimensional Arrays. *Science* **1997**, *276*, 233-235.

[27]   Choi, I. S.; Weck, M.; Xu, B.; Jeon, N. L.; Whitesides, G. M. Mesoscopic, Templated Self-Assembly at the Fluid-Fluid Interface. *Langmuir* **2000**, *16*, 2997-2999.

[28]   Huck, W. T. S.; Tien, J.; Whitesides, G. M. Three-Dimensional Mesoscale Self-Assembly. *J. Am. Chem. Soc.* **1998**, *120*, 8267-8268.

[29]   Clark, T. D.; Boncheva, M.; German, J. M.; Weck, M.; Whitesides, G. M. Design of Three-Dimensional, Millimeter-Scale Models for Molecular Folding. *J. Am. Chem. Soc.* **2002***, 124*, 18-19.

[30]   Clark, T. D.; Tien, J.; Duffy, D. C.; Paul, K. E.; Whitesides, G. M. Self-Assembly of 10-μm-Sized Objects into Ordered Three-Dimensional Arrays. *J. Am. Chem. Soc.* 2001*, 123*, 7677-7682.

[31]   Gracias, D. H.; Tien, J.; Breen, T. L.; Hsu, C.; Whitesides, G. M. Forming Electrical Networks in Three Dimensions by Self-Assembly. *Science* **2000***, 289*, 1170-1172.

[32]   Fernandes, R.; Gracias, D. H. Self-folding polymeric containers for encapsulation and delivery of drugs. *Adv. Drug Deliv. Rev.* **2012***, 64*, 1579-1589.

[33]   Randall, C. L.; Gultepe, E.; Gracias, D. H. Self-folding devices and materials for biomedical applications. *Trends Biotechnol.* **2011***, 30*, 138-146.

[34]   Leong, T. G.; Zarafshar, A. M.; Gracias, D. H. Patterning: Three-Dimensional Fabrication at Small Size Scales. *Small* **2010***, 6*.

[35]   Lu, Y.; Kim, C. Microhand for biological applications. *Appl. Phys. Lett.* **2006***, 89*, 164101.

[36]   Iwase, E.; Shimoyama, I. Multistep sequential batch assembly of three-dimensional ferromagnetic microstructures with elastic hinges. *Microelectromechanical Systems, Journal of* **2005***, 14*, 1265-1271.

[37]   In, H. J.; Lee, H.; Nichol, A. J.; Kim, S.; Barbastathis, G. Carbon nanotube–based magnetic actuation of origami membranes. *Journal of Vacuum Science & Technology B* **2008***, 26*, 2509-2512.

[38]   M Shahinpoor and Y Bar-Cohen and J O Simpson and,J.Smith Ionic polymer-metal composites (IPMCs) as biomimetic sensors, actuators and artificial muscles - a review. *Smart Mater. Struct.* **1998***, 7*, R15.

[39]   Guan, J.; He, H.; Hansford, D. J.; Lee, L. J. Self-Folding of Three-Dimensional Hydrogel Microstructures. *J Phys Chem B* **2005***, 109*, 23134-23137.

[40]   Luo, J. K.; Huang, R.; He, J. H.; Fu, Y. Q.; Flewitt, A. J.; Spearing, S. M.; Fleck, N. A.; Milne, W. I. Modelling and fabrication of low operation temperature microcages with a polymer/metal/DLC trilayer structure. *Sensors and Actuators A: Physical* **2006***, 132*, 346-353.

[41]   Suzuki, K.; Yamada, H.; Miura, H.; Takanobu, H. Self-assembly of three dimensional micro mechanisms using thermal shrinkage of polyimide. *Microsystem Technologies* **2007***, 13*, 1047-1053.

[42]   Syms, R. R. A.; Yeatman, E. M.; Bright, V. M.; Whitesides, G. M. Surface tension-powered self-assembly of microstructures - the state-of-the-art. *Microelectromechanical Systems, Journal of* **2003***, 12*, 387-417.

[43]   Randall, C. L.; Leong, T. G.; Bassik, N.; Gracias, D. H. 3D lithographically fabricated nanoliter containers for drug delivery. *Adv. Drug Deliv. Rev.* **2007***, 59*, 1547-1561.

[44]   Randall, C.; Gillespie, A.; Singh, S.; Leong, T.; Gracias, D. Size selective sampling using mobile, 3D nanoporous membranes. *Analytical and Bioanalytical Chemistry* **2009***, 393*, 1217-1224.

[45]   Ye, H.; Randall, C.; Leong, T.; Slanac, D.; Call, E.; Gracias, D. Remote Radio-Frequency Controlled Nanoliter Chemistry and Chemical Delivery on Substrates. *Angewandte Chemie* **2007***, 119*, 5079-5082.

[46]   Gimi, B.; Artemov, D. F.; Leong T FAU - Gracias, David,H.; FAU, G. D.; Gilson, W. F.; Stuber M FAU - Bhujwalla, Zaver,M.; Bhujwalla, Z. M. Cell viability and noninvasive in vivo MRI tracking of 3D cell encapsulating self-assembled microcontainers. *Cell transplantation JID - 9208854* **1226**.

[47]   Leong, T. G.; Lester, P. A.; Koh, T. L.; Call, E. K.; Gracias, D. H. Surface Tension-Driven Self-Folding Polyhedra. *Langmuir* **2007***, 23*, 8747-8751.

[48]   Pandey, S.; Ewing, M.; Kunas, A.; Nguyen, N.; Gracias, D. H.; Menon, G. Algorithmic design of self-folding polyhedra. *Proceedings of the National Academy of Sciences* 2011*, 108*, 19885-19890.

[49]   J. A. Castellano, *Handbook of display technology*, Academic Press, San Diego, **1992**.

[50]   G. P. Crawford, *Flexible Flat Panel Displays*, John Wiley & Sons, **2005**.

[51]   H. Zhang, M. Sakakura, H. Kuwabara. Electronic device having an active matrix display panel. *U.S. Patent No.* US6462806B2, **2001**.

[52]   Estevez, L.; Moizio, F.; DuVal, M.; Bommersbach, W. Wireless display. *U.S. Patent No.* 20030017846A1, **2003**.

[53]   Kerr, D. Wireless display for electronic devices. *U.S. Patent No.* US20130084796A1, **2013**.

[54] Leong, T.; Gu, Z.; Koh, T.; Gracias, D. H. Spatially Controlled Chemistry Using Remotely Guided Nanoliter Scale Containers. *J. Am. Chem. Soc.* **2006**, *128*, 11336-11337.

[55] Paul, D. R.; McSpadden, S. K. Diffusional release of a solute from a polymer matrix. *J. Membr. Sci.* **1976**, *1*, 33-48.

[56] Gutowska, A.; Bae, Y. H.; Feijen, J.; Kim, S. W. Heparin release from thermosensitive hydrogels. *J. Controlled Release* **1992**, *22*, 95-104.

[57] Patel, V.; Amiji, M. Preparation and Characterization of Freeze-dried Chitosan-Poly(Ethylene Oxide) Hydrogels for Site-Specific Antibiotic Delivery in the Stomach. *Pharm. Res.* **1996**, *13*, 588-593.

[58] Kost, J.; Leong, K.; Langer, R. Ultrasound-enhanced polymer degradation and release of incorporated substances. *Proceedings of the National Academy of Sciences* **1989**, *86*, 7663-7666.

[59] D'Emanuele, A.; Staniforth, J. An Electrically Modulated Drug Delivery Device: I. *Pharm. Res.* **1991**, *8*, 913-918.

[60] Hsieh, D. S.; Langer, R.; Folkman, J. Magnetic modulation of release of macromolecules from polymers. *Proc. Natl. Acad. Sci. U. S. A.* **1981**, *78*, 1863-1867.

[61] Nolan, C. M.; Serpe, M. J.; Lyon, L. A. Thermally Modulated Insulin Release from Microgel Thin Films. *Biomacromolecules* **2004**, *5*, 1940-1946.

[62] Ma, M.; Zhu, Y.; Li, L.; Cao, S. Nanostructured porous hollow ellipsoidal capsules of hydroxyapatite and calcium silicate: preparation and application in drug delivery. *J. Mater. Chem.* **2008**, *18*, 2722-2727.

[63] Kalinin, Y. V.; Randhawa, J. S.; Gracias, D. H. Three-Dimensional Chemical Patterns for Cellular Self-Organization. *Angewandte Chemie International Edition* **2011**, *50*, 2549-2553.

[64]   Kalinin, Y. V.; Randhawa, J. S.; Gracias, D. H. Three-Dimensional Chemical Patterns for Cellular Self-Organization. *Angewandte Chemie* **2011***, 123*, 2597-2601.

[65]   Le, H. P., Progress and trends in ink-jet printing technology. Journal of Imaging Science and Technology **1998**, 42 (1), 49-62.

[66]   Lipson, H., Kurman, M. , *Fabricated: The new world of 3D printing.* John Wiley & Sons: **2013**.

[67]   Mannoor, M. S.; Jiang, Z.; James, T.; Kong, Y. L.; Malatesta, K. A.; Soboyejo, W. O.; Verma, N.; Gracias, D. H.; McAlpine, M. C., 3D Printed Bionic Ears. *Nano Letters* **2013**, 13 (6), 2634-2639.

[68]   Showalter, K. Trigger waves in the acidic bromate oxidation of ferroin. *J. Phys. Chem.* **1981***, 85*, 440-447.

[69]   Wood, V.; Panzer, M. J.; Chen, J.; Bradley, M. S.; Halpert, J. E.; Bawendi, M. G.; Bulović, V., Inkjet-Printed Quantum Dot–Polymer Composites for Full-Color AC-Driven Displays. *Advanced Materials* **2009**, 21 (21), 2151-2155.

[70]   Lee, H. –H.; Chou, K. –S., Inkjet printing of nanosized silver coloids. *Nanotechnology* **2005***, 16*, 2436.

CURRICULUM VITAE

Jinpyo Hong
1 E University Pkwy Unit 705, Baltimore, MD 21218
Cell: (425) 829-7980
E-mail: jhong33@jhu.edu

· Education

JOHNS HOPKINS UNIVERSITY (JHU)	Baltimore, MD
Master of Science in Chemical and Biomolecular Engineering	May 2015

Bachelor of Science in Chemical and Biomolecular Engineering	May 2014

Interfaces and Nanotechnology Concentration

Relevant Coursework: Micro/Nanotechnology, Micro/Nano Structured Materials & Devices, Introduction to Polymeric Materials, Chemical Engineering Lab; Chemical and Biological Process Analysis, Thermodynamics, Transport Phenomena

· Work Experience

Johns Hopkins University (JHU)
Gracias Laboratory, Department of Chemical and Biomolecular Engineering   Baltimore, MD
Graduate Researcher / Research Assistant   2011 – 2015

- Conducted multiple research projects related to nano & micro technology and assisted graduate students.
- Previous research themes include: fabrication of nanostructure and directed self-assembly of micro and nanoscale structures, and uniform & non-uniform diffusion process of chemicals from nanoscale structures and more.
- Acquired extensive hands on experience on microfabrication with a strong record of problem solving and productivity with significant achievements (see below).

Highlights of Achievements
1. Peer Reviewed Journal Publication
Y.V. Kalinin[*], S. Pandey[*], **J. Hong** and D. H. Gracias, A chemical display: Generating animations by controlled diffusion from porous voxels, *Advanced Functional Materials* (**2015**), accepted.

2. Presentation at National Workshops
S. Pandey, **J. Hong** and D. H. Gracias, Patterning chemistry in an array of BZ reaction systems, NSF Building Engineered Complex System (BECS) Workshop, Arlington, VA (**2013**).

3. Patent
Y.V. Kalinin[*], S. Pandey[*], **J. Hong** and D. H. Gracias[*], A Dynamical Display Based on Chemical Release from Printed Porous Voxels, Provisional patent application filed (**2015**).

4. Oral Presentations
"Directional Assembly of Patterned Polyhedral Patchy Particles", Spring 2014
"BZ Reaction in a Non-Uniform Medium", Fall 2013
"BZ Reaction: Dependence of Chemical Pattern Generation on Geometry and Boundary Conditions", Fall 2012
"Chemical Release: Uniform Diffusion from Microscale Containers", Spring 2011

· Skills & Laboratory Techniques

- Microfabrication: Clean room protocols, photolithography, soft lithography, electroplating, vapor deposition, metallic and polymeric nanoparticles, wet and plasma etching, self-assembly of metallic micro/nanoparticles and molding.
- Imaging: Optical and Fluorescence Microscopy
- Multiple programs including Microsoft Office, Adobe Photoshop, Illustrator and InDesign, MATLAB and AutoCAD